NIH Public Access
Author Manuscript
Vision Res. Author manuscript; available in PMC 2012 July 1.

Published in final edited form as:
Vision Res. 2011 July 1; 51(13): 1379–1396. doi:10.1016/j.visres.2011.05.002.

Imaging Single Cells in the Living Retina

David R. Williams
Director, Center for Visual Science, William G. Allyn Professor of Medical Optics, University of Rochester, Box 270270, Rochester, New York 14627-0270, TEL 585 275-8672, FAX 585 271-3043

David R. Williams: david@cvs.rochester.edu

Abstract

A quarter century ago, we were limited to a macroscopic view of the retina inside the living eye. Since then, new imaging technologies, including confocal scanning laser ophthalmoscopy, optical coherence tomography, and adaptive optics fundus imaging, transformed the eye into a microscope in which individual cells can now be resolved noninvasively. These technologies have enabled a wide range of studies of the retina that were previously impossible.

Keywords

retinal imaging; confocal scanning laser ophthalmoscope; adaptive optics; optical coherence tomography; spatial resolution; ophthalmoscopy

The ability to look inside the living human eye is central to our understanding of how the normal eye works and the diseased eye fails. This article focuses on technological advances in the spatial resolution of retinal imaging during the last quarter century and some of the scientific discoveries they have made possible. These advances have transformed retinal imaging from a macroscopic to a microscopic modality in which individual cells can now be resolved. There are many books and review articles that address these advances. Relevant books include (Huang et al., 2006; Masters, 2001; Porter et al, 2006; Schulman et al., 2004) and review articles include (Costa, et al., 2006; Drexler and Fujimoto, 2008; Fujimoto, 2003; Godara et al., 2010; Hampson, 2008; Miller et al., 2011; Miller and Roorda, 2009; Mojtkowski, 2010; Podoleanu, 2005; Podoleanu and Rosen, 2008; Roorda, 2010; Rossi et al. 2011; and Wilt et al., 2009).

It has never been easy to peer inside the living eye. Though several investigators in the 19th century were aware of the illumination conditions necessary to cause the otherwise impenetrable pupil to glow red, they failed to obtain a clear view of the living retina until Helmholtz invented the ophthalmoscope (Helmholtz, 1851). Since then, the evolution of this instrument has been punctuated by important, if occasional, technical advances such as adding a camera that could record retinal images on film (Jackman and Webster, 1886).

© 2011 Elsevier Ltd. All rights reserved.

Corresponding Author: David Williams.

Conflict of Interest Disclosure: My employer, the University of Rochester, holds intellectual property on which I am an inventor and that pertain to the subject matter of this article.

Publisher's Disclaimer: This is a PDF file of an unedited manuscript that has been accepted for publication. As a service to our customers we are providing this early version of the manuscript. The manuscript will undergo copyediting, typesetting, and review of the resulting proof before it is published in its final citable form. Please note that during the production process errors may be discovered which could affect the content, and all legal disclaimers that apply to the journal pertain.

NIH-PA Author Manuscript
NIH-PA Author Manuscript
NIH-PA Author Manuscript

NIH-PA Author Manuscript

NIH-PA Author Manuscript

NIH-PA Author Manuscript

Surprisingly, before the late 1980's there were few improvements in optical resolution since Helmholtz's landmark invention. A rare example is the incorporation of the electronic flash, invented ~30 years earlier by Edgerton, that allowed exposures brief enough to avoid eye motion blur (Ogle and Rucker, 1953). In contrast, the last quarter century has witnessed gains in spatial resolution that have completely transformed our capacity to recover information from the retinal image.

The first glimpses of retinal cells in the living eye

The fact that ophthalmoscopy lacked the resolution to see single cells a quarter of a century ago did not preclude drawing inferences about the effects of single cells on vision well before then. Perhaps the best example is the brilliant paper of Hecht, Schlaer, and Pirenne (1941) in which they concluded that ~10 photons are required to detect a flash at absolute threshold. Because these 10 quantal absorptions almost certainly occurred in 10 different receptors, they could conclude that absorption of one photon of light was sufficient to excite a single rod. Their argument was necessarily a statistical one because the poor optical quality of the eye precludes stimulating one and only one rod in the human eye. However, there is another class of photoreceptor, the short wavelength sensitive cones, that are rare enough in the retina that a focused point source, suitably arranged to stimulate only that class of cell, can stimulate only one cell at a time. Capitalizing on this unique aspect of this cone submosaic, Don MacLeod, Mary Hayhoe and I (Williams et al., 1981) showed that subjects could reliably detect a flash of light that stimulated a single cone photoreceptor.

These experiments lead to psychophysical methods to characterize the arrangement and spacing of cones that relied on aliasing effects caused by imaging interference fringes on the retina (Williams, 1985; 1988). Artal and Navarro (1989) wondered whether another variant of interferometry, based on the interference of light returning from the retina rather than light entering the eye, could be used to estimate the spacing of cones in the living eye. Their approach was derived from a technique used in astronomy, stellar speckle interferometry, that had been developed to recover high spatial frequency information from speckled images, such as whether an object in the sky was a single or a binary star (Labeyrie, 1970), They collected images of the speckle patterns generated by illuminating small patches of living human retina with coherent light. The average power spectrum of multiple images revealed a ring corresponding to spatial frequency components of the cone mosaic, providing the first evidence about the granularity of the cone mosaic obtained from images of the living human eye.

Unfortunately, Artal and Navarro's method did not allow for the direct observation of the cone mosaic because the cones are obscured by the interference of the coherent light reflected from multiple layers of the retina. Experiments in animals had previously demonstrated direct imaging of receptors. In 1985, Land and Snyder (1985) showed in the snake and Jagger (1985) showed in the cane toad that it is possible to image photoreceptor cells through the natural optics of the intact eye. While these observations were made on animal eyes with good optics and unusually large receptors, they encouraged the possibility that this could also be achieved in the human eye. Cidecyian and Jacobson (1994) noticed small bright spots in fundus images from patients who were carriers of x-linked retinitis pigmentosa. They speculated that these spots were cones back-illuminated by the highly-reflective tapetum-like fundus in these patients.

Miller et al. (1996) constructed a custom fundus camera specifically designed to search for single cones in the normal human eye. This camera illuminated the retina with a small, ~7 minutes of arc, field of monochromatic light. To avoid speckle, the laser source used was deliberately rendered incoherent with a spinning diffuser. Careful attention was paid to the

NIH-PA Author Manuscript

NIH-PA Author Manuscript

NIH-PA Author Manuscript

correction of defocus and astigmatism. With this instrument they obtained the first direct images of the cone mosaic in the normal living human eye, examples of which are shown in Fig. 1. Cones continue to be a favorite target for retinal microscopy because they act like tiny waveguides, and the light that enters them is preferentially redirected back through the pupil, producing a high contrast mosaic of bright spots in the retinal image. There is a common misconception that additional optical techniques such as adaptive optics are required to image the cone mosaic in the living eye, but Miller et al. showed, and many others have since confirmed (eg. Wade and Fitzke, 1998; Vohnsen, Iglesias, and Artal, 2004, Pircher, Baumann, Gotzinger, and Hitzenberger, 2006), that cellular imaging is possible outside the foveal center in young eyes with good optical quality and careful correction of defocus and astigmatism alone. These early glimpses of structures as small as single cones in the living human eye encouraged the development of new technologies, especially adaptive optics, to improve the resolution of retinal imaging.

The scanning laser ophthalmoscope

The invention of the scanning laser ophthalmoscope (SLO) by Webb, Hughes, and Pomerantzeff (1980) represented a radical departure from the design of conventional fundus cameras of the time and laid the groundwork for modern retinal microscopy. They developed what they called initially a “flying spot TV ophthalmoscope” that raster-scanned a single laser spot onto the retina, collecting the returning light onto a detector with much greater sensitivity than film. The use of a dilated pupil to collect the light and a photomultiplier tube for light detection made it possible to collect video images of the retina with significantly less light exposure than the conventional film-based fundus cameras of the time. In 1987, Webb, Hughes, and Delori introduced the principle of confocal detection into an improved SLO. Marvin Minsky (1957), better known for his contributions to artificial intelligence, first proposed the idea of confocal imaging in a patent for a scanning microscope. Surprisingly, it took 30 years for this simple and effective principle to find its way from microscopy into ophthalmoscopy. The confocal SLO used the same optical path for scanning the laser spot on the retina and for delivering the returning light to the detector, as shown in Fig. 2. This double passage of light through the scanning mirrors produced a stable image at the detector of the scanned spot on the retina. A confocal pinhole just in front of the light detector collected most of the light from the retina while rejecting light originating from planes other than the retina. Though the instrument did not improve lateral resolution over that which could be achieved with conventional fundus cameras of the day, it did improve axial resolution, significantly increasing image contrast. As shown in Fig. 3, the axial resolution of the confocal SLO was about 300 microns, modest by today's standards, but it represented the first improvement in resolution since the flash tube prevented eye motion blur. Moreover, the scanning technology and confocal detection method introduced by Webb and his colleagues were key elements of many of the high resolution, microscopic retinal imaging technologies that were soon to follow.

Improvements in axial resolution through OCT

The fundus cameras and confocal SLOs circa 1990 were designed on the premise that light is made of particles that travel in straight lines. Though the wave nature of light had been proposed by Huygens in 1678 and confirmed by Thomas Young's famous double slit interference experiment in 1804, it had yet to impact methods to image the retina. But in the 1990's, optical coherence tomography harnessed the wave nature of light, thereby achieving an unprecedented axial resolution in retinal images. The retina is a 3 dimensional structure from 100-400 microns thick that is organized into distinct layers of cells and the synaptic connections between them. Each layer has a specific role in the circuitry that transforms the retinal image into signals the brain can interpret, and each can be affected differently in

NIH-PA Author Manuscript

NIH-PA Author Manuscript

NIH-PA Author Manuscript

retinal disease. OCT provided for the first time a high-resolution cross-sectional view through the living retina, comparable to a histological section but without requiring retinal excision. It is important to emphasize that OCT did not just provide an increase in resolution; it literally provided a view of the living retina that was previously completely inaccessible. This feature and the fact that it is a relatively robust technology helped it gain the widespread use it enjoys today.

The idea had been around since the early 1970's that one might recover the depth profile of thick tissue from the variation in the time it takes for light to return from different depths. But the speed of light is so high that this is not practical to measure, and the early pioneers of OCT seized instead on low coherence interferometry. The historical roots of low coherence interferometry lay in the observation by Robert Hooke in 1664 that interference could be observed between two reflective surfaces illuminated in white light. This phenomenon was later analyzed by Isaac Newton, and became known as “Newton's rings”. The basic principle of marshalling low coherence to measure depth profiles in the eye is shown in Fig. 4a, in the context of what is now called time domain OCT. A light source is used that has very short coherence length, ideally small compared with the retinal layers one wishes to distinguish. This short coherence length implies that when the beam is split in two by a fiber coupler and one beam is directed at the retina and the second one to a reference mirror, the two beams, when brought back together, can only interfere if the two beams traveled the same optical path length to within the coherence length of the source. Shifting the axial position of the reference mirror changes the depth in the retina where interference can be produced, and the magnitude of the interference signal at that depth increases with the intensity of the reflection. By measuring the magnitude of the interference signal as a function of the axial position of the reference mirror, it is possible to identify the light reflected from different depths, without the need to measure the transit time of light. The earliest application of these ideas to the eye produced a depth profile along a line passing through a single point on the retina, allowing, for example, very precise measurements of the axial length of the eye (eg. Fercher et al.,1988). By transverse scanning, sequentially acquiring axial depth profiles along a linear series of locations across the retina, one can construct a 2 dimensional tomograph or retinal cross-section in the living eye. OCT is able to detect much weaker signals from the retina than conventional fundus imaging because it takes advantage of the increased gain provided by heterodyne detection. In heterodyne detection, the amplitude of the interference signal is proportional to the product of the amplitudes of the two interfering beams so that the use of a large amplitude reference beam amplifies the weak interference signal. David Huang and colleagues, working in Jim Fujimoto's laboratory at MIT, made the first in vitro optical coherence tomograph of the retina in 1991 (Huang, 1991). Adolph Fercher's group made the first in vivo optical coherence tomography of the optic disc in 1993 (Fercher et al., 1993).

The next major step in the evolution of OCT was to improve the axial resolution even further. The first systems had a fairly long coherence length, which provided a theoretical resolution of about 10-15 microns. In 1999, Wolfgang Drexler, working in Jim Fujimoto's lab, pioneered the use of broader band, shorter coherence length, sources that could in principle achieve an axial resolution of 3 microns in the eye, two orders of magnitude better than the confocal SLO. Though the resolution improvement is limited to a single spatial dimension, ultrahigh resolution OCT could in theory produce a point spread function in the axial dimension smaller than the size of many cells in the retina.

A major limitation of time-domain OCT is the speed at which the retina can be scanned. This is especially problematic because large movements of the eyes could occur even with the fastest scanning speeds available. The main limitation on the speed of image acquisition in time domain OCT is the time required to shift the optical path length in the reference arm

NIH-PA Author Manuscript

NIH-PA Author Manuscript

NIH-PA Author Manuscript

of the interferometer, either through mechanical displacement of the mirror or a variable delay line. Avoiding this delay, Fercher introduced the basic principle of spectral domain OCT in 1995. A typical layout for a spectral domain OCT is shown in Fig. 4b. It is similar to the time domain OCT with the exception of the detection arm of the system, which contains a spectrometer instead of a simple light detector. The spectrometer consists of a diffraction grating and a one-dimensional CCD that can acquire the entire spectrum of the light returning from a single retinal location in parallel. Spectral domain OCT obviates the need for scanning in the reference arm to acquire the depth profile at each retinal location. Instead, the reflectance at each depth is obtained from variations in the pattern of interference across the spectrum of the reflected light. The spectrum contains depth information because the light reflected from a single depth at one retinal location will generally produce a sinusoidal variation in the interference pattern across wavelength. The amplitude of this sinusoid is proportional to the square root of the amplitude of the electric field reflected at that point. The frequency of this sinusoid increases as the optical path length difference between the reference and sample increases. Therefore, the Fourier transform of the spectrum of the light returning from reflection will reveal the amount of light reflected at each axial depth at that retinal location. The first demonstration of its application in retinal imaging was published in 2002 (Wojtkowski et al., 2002a, b). The introduction of spectral domain OCT (sometimes called Fourier or frequency domain OCT) increased the sensitivity of OCT by roughly 2 orders of magnitude. The reason for this improvement is because, in time-domain OCT, at any instant, all the light is lost that is illuminating other retinal layers than the one that happens to be interfering with the reference arm. In spectral domain OCT, at any instant, light from all retinal layers contribute to defining the axial profile. An example of a spectral domain OCT scan from Jack Werner's group at UC, Davis is shown in Fig. 5.

Swept source OCT is a related method that also generates the depth profile through spectral information. In swept source OCT, the wavelength of the light source is rapidly swept to obtain the necessary spectral information to compute the depth profile at each retinal location (Choma et al., 2003). The layout of a swept source OCT system is shown in Fig. 4c. Many groups are now acquiring three-dimensional volumes of the retina with these methods (eg. Drexler and Fujimoto, 2008). These evolving technologies have revolutionized retinal imaging in ophthalmology and two decades after the introduction of the first time domain OCT systems, they are ubiquitous tools in the eye clinic. Though OCT offers a 100-fold improvement in axial resolution over the confocal SLO and is even better still in that dimension than the conventional fundus camera, it does not improve provide any resolution gains in either of the other two lateral spatial dimensions. Fortunately, a way to improve lateral resolution was also under development in the 1990s.

Improvements in Lateral Resolution Through Adaptive Optics

The quality of fundus cameras is typically good enough that the lateral resolution is limited not by the instrument but by the optical quality of the human eye. The limitations in eyes with relatively good optics include diffraction by the eye's pupil and aberrations, with light scatter becoming a significant source of blur in older eyes and young eyes with unusually cloudy optics. The effects of diffraction and aberrations on the eye's point spread function are illustrated in Fig. 6. When both diffraction and aberrations are present, the optimum pupil diameter is in the range of 2-3 mm. If diffraction were the only source of image blur, then for microscopic imaging there would be a clear advantage of using the largest pupil possible. In theory, retinal imaging without any aberrations and a pupil fully dilated to 8 mm could produce a point spread function with a full width at half height as small as 1.4 microns in the middle of the visible spectrum. Unfortunately, in the typical eye, aberrations corrupt the point spread function at large pupil diameters, removing most of the benefit of escaping

NIH-PA Author Manuscript

NIH-PA Author Manuscript

NIH-PA Author Manuscript

diffraction. Full aberration correction with an 8 mm pupil could provide a 3.4-fold gain in lateral resolution over that obtained with a 2.5 mm entrance pupil. This benefit applies to two spatial dimensions, reducing the 3-d volume of the PSF by a factor of ~10. This benefit in lateral resolution does not include the potential benefit in axial resolution that can be achieved by correcting aberrations to be discussed later.

In conventional fundus cameras designed for wide field clinical imaging, no attention is usually paid to correcting aberrations other than defocus. But if the goal is to maximize the lateral resolution of microscopes for imaging the living retina at a cellular spatial scale, it is necessary to compensate not only for defocus, but also astigmatism and a host of other aberrations that we now refer to as higher order aberrations. A quarter of a century ago, higher order aberrations were collectively called “irregular astigmatism”. Only a few devoted disciples of physiological optics had succeeded in characterizing some of the individual aberrations that make up irregular astigmatism, and because no method existed to correct them, the importance of their work went largely unrecognized. Smirnov (1961) used a subjective vernier task to measure the third- and fourth-order aberrations of the eye. He lamented the lengthy calculations required to compute the wave aberration and stated that it was unlikely this method would have practical significance, not foreseeing the rapid increase in computing speed that would make it possible within 40 years to measure and compute the eye's wave aberration in a few tens of milliseconds. Walsh, Charman, and Howland (1984) demonstrated the first objective method to measure the eye's wave aberration. This was a significant breakthrough in the history of aberration measurement, but the method was never widely adopted because it was never automated.

Junzhong Liang, working as a graduate student in Josef Bille's laboratory at the University of Heidelberg demonstrated that it was possible to adapt for use in the eye the Shack–Hartmann wavefront sensor that is widely used in astronomical adaptive optics (Liang et al., 1994). Liang joined my laboratory at the University of Rochester to develop a high-resolution wavefront sensor that provided a more complete description of the eye's wave aberration, measuring up to 10 radial Zernike orders (Liang and Williams, 1997). The Shack-Hartmann wavefront sensor was eventually automated in a collaborative effort between Pablo Artal's group at the University of Murcia and my group at Rochester (Hofer et al., 2001). The automation of wavefront sensing and the promise of correcting higher order aberrations with laser refractive surgery lead to rapid commercialization. Even though some of the eye's higher order aberrations had been measured in various clever ways for more than 40 years, their significance for vision correction and high resolution retinal imaging was not widely recognized until adaptive optics was used successfully to correct them.

Early adaptive optics systems for the eye

The wave aberration is unique in every eye and it is dynamic over time, largely due to fluctuations in focus (Hofer et al., 2001). Therefore, the correction of the wave aberration requires an optical element that could assume an essentially infinite number of possible shapes over time. Fortunately, just such a technology had been developed to solve a related problem in the field of astronomy. The idea of adaptive optics was first introduced by Horace Babcock (1953), who suggested that an adaptive optical element could remove the blur in stellar images from the time-varying aberrations produced by the turbulent atmosphere. Babcock was unable to implement his idea at the time because the technology did not exist to measure and correct the aberrations he could see dancing just out of reach in the pupil plane of his telescope. In 1977, Hardy and his colleagues succeeded in the first empirical demonstration of adaptive optics in astronomy. Now adaptive optics is commonplace among the best ground-based telescopes around the world.

NIH-PA Author Manuscript

NIH-PA Author Manuscript

NIH-PA Author Manuscript

In 1989, Andreas Dreher, working in Joseph Bille's laboratory at the University of Heidelberg, used a deformable mirror to improve retinal images in a scanning laser ophthalmoscope (Dreher et al, 1989), correcting the astigmatism in one subject's eye based on a conventional spectacle prescription. At the time, Bille's group had not yet developed the Shack-Hartmann wavefront sensor, so that they were not able to correct additional aberrations beyond astigmatism.

Junzhong Liang, Don Miller, and I constructed the first closed-loop adaptive optics system that could correct higher order aberrations in the eye, shown in Fig. 7 (Liang et al, 1997). The system consisted of a Shack-Hartmann wavefront sensor to measure the eye's aberrations, a 37 actuator deformable mirror to correct the aberrations, and a flash-illuminated fundus camera to acquire a retinal image once the eye's aberrations had been compensated through the AO control loop. This first system required about 15 min for each loop of measuring and correcting the wave aberration, with 4 or 5 loops required to complete the correction. As slow as this system was, it could produce better images of the cone mosaic than Miller had previously obtained without adaptive optics. Real time, automated adaptive optics systems soon followed (Hofer, 2001b; Fernandez et al., 2001).

Color vision and the trichromatic cone mosaic

Shortly after the AO fundus camera was developed, it was applied to the problem of imaging the trichromatic organization of the cone mosaic in the human retina. Though it had been known for nearly 200 years that human color vision relies on three channels each tuned to a different part of the visible spectrum (Young 1801), the arrangement and relative numbers of all three cone classes in the human eye had not been subject to direct scrutiny. Austin Roorda, then a postdoc at the University of Rochester, combined retinal densitometry (Campbell and Rushton, 1955) with adaptive optics, making it possible to reliably identify the photopigment in single cones throughout large patches of cones near the foveal center (Roorda and Williams, 1999, Roorda et al., 2001).

The signal to noise ratio of single images of the cone mosaic was too poor to reliably identify the pigment contained in each cone. This made it necessary to add many images. Eye movements that occurred between frames are typically many times larger than the diameter of a cone, so that it was necessary to register multiple frames with cross-correlation before adding them. This approach turned out to be effective at increasing signal-to-noise ratio without compromising image quality through registration error. Putnam et al. (2005) later showed that it is possible to record the retinal location of a fixation target on discrete trials with an error at least 5 times smaller than the diameter of the smallest foveal cones. These results showed how accurate this process could be, and that registration error with high quality AO images can be smaller than the point spread function of the aberration corrected image. The ability to register and add such high spatial resolution images turns out to be key to microscopic retinal imaging because safety limits often preclude delivering all the light in a single exposure.

The results of Roorda's analysis, and subsequent measurements by Heidi Hofer et al. (2005a) showed that the distribution of the different photopigments in foveal cones is essentially random and revealed directly a very large (40-fold) variation in the relative numbers of L and M cones across individuals. (See Fig. 8). One of the most powerful aspects of the ability to characterize the trichromatic mosaic in the living human eye is that it allows psychophysical measures of visual performance that can be directly correlated with mosaic organization. For example, it allowed experiments that demonstrate that color experience is not affected by the relative numbers of L and M cones (Brainard et al., 2000, Neitz et al., 2002).

NIH-PA Author Manuscript

NIH-PA Author Manuscript

NIH-PA Author Manuscript

Adaptive optics for vision correction

Adaptive optics corrects the wave aberration simultaneously for light entering the eye as well as light leaving the eye. This makes it useful both for vision correction and for retinal imaging. By way of example, it has also allowed experiments in which flashes smaller than single photoreceptors are delivered to the cone mosaic to probe the color experience produced when single cones are stimulated (Hofer et al., 2005b). These experiments showed that cones containing the same photopigment do not always generate the same color appearance, supporting the view that color appearance depends also on the identities of nearby cones (Brainard et al., 2008).

The use of adaptive optics for vision correction has expanded in many exciting new directions, not only for studying vision when aberrations are corrected (e.g. Artal et al., 2010; Atchison et al., 2009a, 2009b; Dalimier & Dainty, 2008; Dalimier et al., 2008; de Gracia et al., 2010; Elliott et al., 2009; Guo & Atchison, 2010; Gupta et al., 2010; Li, J. et al., 2009; Li, S. et al., 2009; Liang et al., 1997; Lundstrom et al., 2007; Marcos et al., 2008; Perez et al., 2009; Rocha et al., 2007, 2010; Rossi and Roorda, 2010; Rossi et al., 2007; Rouger et al., 2009; Sawides et al., 2010; Williams et al., 2000; Yoon & Williams, 2002). Adaptive optics can be used to study visual performance by generating specific novel aberration patterns in the eye (e.g. Chen et al. 2005). This use of adaptive optics has revealed that the nervous system has adapted to the specific pattern of aberrations in the eye (Artal, et al., 2003; Chen et al., 2007; Sabesan and Yoon, 2010; Atchison and Guo, 2010). AO vision correction systems have also been used to study other aspects of vision such as motion processing (Raghunandan et al., 2008), accommodation (Chen et al., 2006; Fernandez and Artal, 2005; Hampson et al., 2010), and binocular vision (Fernandez et al., 2010). AO may ultimately provide a rapid and highly reliable alternative to the subjective phoropter used to refract the eye.

Genetics and the cone mosaic

Another advantage of in vivo resolution of the human photoreceptor mosaic is that it made it vastly simpler to determine how polymorphisms in the genes that code for the photoreceptors influence the mosaic that is ultimately formed. Joe Carroll and colleagues (Carroll et al., 2004), working initially on the flood-illuminated AO ophthalmoscope at Rochester discovered a new cause for color blindness in which a mutation in the gene for one of the three cone photopigments results in a mosaic of cones that shows patchy loss. (See Fig. 9). Interestingly, despite the loss of nearly 1/3 of the patient's foveal cones, his visual acuity is normal (20/15), indicating that adaptive optics imaging can detect retinal degeneration well before conventional clinical tests. Carroll and colleagues have gone on to describe the mosaic phenotype of an impressive number of different polymorphisms (Baraas et al., 2007; Carroll et al., 2009; Carroll et al., 2010, Wagner-Schuman et al., 2010).

Adaptive Optics Scanning Laser Ophthalmoscopy

The adaptive optics fundus camera built at the University of Rochester had a greatly improved lateral resolution over cameras without AO but it had effectively no axial sectioning, which meant that scattered light throughout the eye and instrument could reduce image contrast (see Fig. 3). But even the confocal SLOs of the 1980s had a axial sectioning capable of removing corneal and lenticular scatter though, at about ~300 microns, not enough to provide much useful optical sectioning of the retina.

Austin Roorda, then at the University of Houston, and his colleagues built the first instrument that combined the benefits of adaptive optics with those of the confocal SLO (Roorda et al., 2002). The optical layout of an AOSLO is shown in Fig. 10. This new

NIH-PA Author Manuscript

NIH-PA Author Manuscript

NIH-PA Author Manuscript

instrument had a number of important advantages. First, adaptive optics increased confocality by increasing the quality of the retinal image at the pinhole, allowing the use of smaller pinholes and therefore better rejection of light from unwanted planes away from the image plane. The sectioning capability of the AOSLO is shown in Fig. 11 (see also, Fig. 3). In the most recent AOSLOs at the University of Rochester, this has improved the axial resolution of the first confocal SLOs by about an order of magnitude. Second, the AOSLO provides microscopic resolution with a real-time view of the retina. This has enabled the video-rate imaging of the motion of individual blood cells in the smallest capillaries in the retina (Martin and Roorda, 2005; Martin and Roorda, 2009; Zhong et al., 2008; Zhong et al., 2011). Tam et al., 2010 has improved the imaging of retinal vasculature without the need for fluorescein by using motion contrast to identify vessels, setting the stage for automated measurements of leukocyte velocity (Tam et al., in press). In vivo studies of blood flow in these smallest of vessels may provide valuable information about early vascular changes in diseases such as diabetic retinopathy.

The clinical utility of AO imaging is only now beginning to be explored (Baraas et al., 2007; Bhatt et al., 2010; Carroll et al., 2004, 2009, 2010; Choi et al., 2006; Chen et al., 2010; Hammer et al., 2008; McAllister et al., 2010; Talcott et al., 2010; Wolfing et al., 2006; Yoon et al., 2009). An exciting recent paper has also shown the potential of AO in drug development (Talcott et al., 2011). They have shown that the AOSLO can detect photoreceptor rescue by a drug, CNTF, in retinitis pigmentosa patients. The value of AO is highlighted by the fact that other standard clinical measures such as visual acuity failed to show a benefit. It seems likely that the microscopic views of cells provided by AO will find their place in the clinic as an especially sensitive indicator of the progression of retinal disease.

In scanning systems such as the SLO, eye movements produce distortion within individual frames as well as translation between frames. The AOSLO is also subject to these distortions, but the increased resolution AO affords allows us to resolve the effects of eye movements at a finer spatial scale. Roorda and collaborators (Stevenson and Roorda, 2005; Vogel et al., 2006) have shown that they can use the warping that occurs in individual frames and between frames in their AOSLO to recover what is probably the most accurate measurement of eye motion ever made. Methods to track the retina with an accuracy approaching the dimensions of single cells will become increasingly important in obtaining enough signal to distinguish subtle changes in retinal cells. Stabilization of the field of view would be especially useful in situations such as microsurgery performed with a microscope equipped with adaptive optics. It is now possible to perform these computations in real time, allowing real-time stabilization of the retinal image for targeted delivery of visual stimuli to the retina (Arathorn et al., 2007; Yang et al., 2010). An alternative approach, under development by Dan Ferguson and Dan Hammer at Physical Sciences Corporation and Steve Burns at Indiana University, is to couple a separate eye tracker to an adaptive optics scanning laser ophthalmoscope for the purposes of image stabilization (Hammer et al., 2006; Burns et al., 2007).

Single unit physiology and single cone inputs to LGN receptive fields

These approaches may herald a new generation of psychophysical experiments in which the location of a stimulus on the retinal cone mosaic can be controlled in real time with an error less than the diameter of a single cone. Indeed, Lawrence Sincich and colleagues (Sincich, 2009) have shown that the AOSLO can be combined with single unit electrical recordings of spike trains in primate lateral geniculate nucleus. Remarkably, as shown in Fig. 12, through exquisite control a point source delivered with AO despite eye movements, they have been able to target and stimulate single cones, recording the responses of LGN cells to light

NIH-PA Author Manuscript

NIH-PA Author Manuscript

NIH-PA Author Manuscript

arriving in single cones. This method will ultimately allow the microdissection of the cone inputs to receptive fields of cells at many stages in the visual pathway in the intact organism.

Imaging the smallest photoreceptors

The performance of adaptive optics systems is steadily improving due to the use of better designs that minimize instrument aberrations (Gomez et al., 2009; Dubra and Salai, in press(), the use of smaller confocal pinholes, and improvements in registration algorithms. Fig. 13a show an image obtained with Alfredo Dubra's AOSLO at the University of Rochester, in which the smallest cones at the foveal center can be resolved. Building on the earlier work of Carroll et al (2008) and Doble et al (2011), Dubra (Dubra et al., in press) can now obtain clear images of single rods in the living human eye (Fig. 13b). Rods are much more difficult than cones to resolve because of their small diameter (~2 microns) and broad angular tuning, which sends less light back through the pupil where it can be collected for imaging. The ability to image rods routinely would be valuable in assessing the progression of retinal degeneration, which often begins with an assault on the rods.

High resolution fluorescence imaging

The introduction of fluorescein angiography revealed the enormous potential of fluorescence retinal imaging for improving the contrast of specific retinal features. The first use of fluorescence in the living human eye was in 1960, when MacLeand and Maumenee used a slit lamp to directly view intravenously-injected fluorescein in the eye (MacLean and Maumenee, 1960). The following year, Novotny and Alvis (1961) combined this method with a fundus camera, collecting the first fluorescein angiograms. Indocyanine green angiography, which provides an enhanced view of blood flow in the choroids was introduced in 1969 (David, 1969). A quarter century ago, these were essentially the only fluorescence methods available in the living eye, but the use of fluorescence has since expanded. An especially exciting example of the resurgence in interest in fluorescence is the recent demonstration of in vivo fluorescence SLO imaging of apoptosis of single primate ganglion cells stained with annexin-5 (Cordeiro et al. 2004). It may someday be possible to track cells on the path to apoptosis in humans with glaucoma. The high contrast provided by fluorescence when only occasional cells are labeled plus the relatively large size of ganglion cells make it easy to resolve these cells without resorting to high resolution methods. Surprisingly, the mouse eye, with a numerical aperture twice that of the human, has a theoretical PSF volume that is 16 times smaller than that of the diffraction-limited human eye. Indeed excellent images of ganglion cells have been obtained in the mouse retina without the need for adaptive optics (Seeliger et al., 2005; Paques, et al. 2006; Walsh and Quigley, 2008; Leung et al., 2008). Melissa Geng at the University of Rochester has recently constructed an AOSLO specifically for the mouse eye, having overcome difficulties in wavefront sensing the mouse optics caused by reflections from multiple retinal layers (Geng et al., 2011). This new instrument promises to reveal subcellular features in the mouse retina never before accessible in the living eye.

Another major new direction in fluorescence imaging began in 1995 when von Ruckmann introduced lipofuscin autofluorescence imaging (von Ruckmann et al, 1995). Lipofuscin is comprised of a number of compounds that are by-products of the visual cycle of photopigment bleaching and regeneration. They accumulate throughout life and are autofluorescent, making it possible to image the retinal pigment epithelium (RPE) for the first time in the living eye. The retinal pigment epithelium lies just behind the photoreceptors and is critically important in servicing them. RPE cells are replete with melanin granules, one role of which is to absorb light that would otherwise scatter and compromise the contrast of the retinal image. But a consequence of this protective role of

NIH-PA Author Manuscript

NIH-PA Author Manuscript

NIH-PA Author Manuscript

melanin is that the RPE cells have relatively low contrast and are difficult to image with reflected light in the living eye (but see Roorda et al., 2007). Autofluorescence imaging was quickly incorporated in commercial instruments, allowing an entirely new view of retinal diseases that compromise the RPE layer.

Imaging RPE cells and ganglion cells with a fluorescence AOSLO

Commercial autofluorescence imaging is achieved with flood-illuminated fundus cameras or confocal SLOs equipped with the appropriate blocking filters. Building on the AOSLO technology introduced by Roorda and colleagues, Dan Gray, Jessica Morgan and others at the University of Rochester added fluorescence imaging capabilities, making it possible to image single RPE cells in the living primate eye (see Fig. 14). The FAOSLO has provided the first *in vivo* images of the RPE cell mosaic in the normal primate eye (Gray et al, 2006; Morgan et al, 2009), taking advantage of the resolution provided by adaptive optics and the AF of lipofuscin inside RPE cells. In a typical frame, the signal measured by the PMT corresponds to only 0.2 photons/pixel, so over a thousand frames are typically averaged to generate an image. Eye motion between successive frames requires image registration before averaging, but the images are too dim to self-register. To overcome this problem, the FAOSLO simultaneously records a high signal-noise-ratio (SNR) movie of the photoreceptors using reflectance imaging in the near infrared and a low SNR fluorescence movie of the RPE in the visible. Since the two movies share the same retinal motion, cross-correlation of cone frames can be used to compute the eye motion correction for the dimmer RPE frames. Discrete RPE cells can be seen because the cell nucleus does not contain lipofuscin and appears dark, whereas the cytoplasm surrounding the nucleus appears bright due to lipofuscin AF.

As shown in Fig. 15, Gray has also shown that it is possible to image ganglion cells including subcellular features such as their dendrites (Gray et al., 2008). The rapid development of fluorescent probes in biology and medicine as well as new methods, such as viral-based methods, to deliver these probes promises to revolutionize retinal imaging. It may soon be possible to image stimulus dependent changes in ganglion cell fluorescence through genetically encoded calcium indicators in the living eye (see Borghuis et al., 2011 for an in vitro demonstration of this approach), which could ultimately clarify why the retina requires 17 or more distinct ganglion cell pathways to convey the retinal image to the brain. To date, in vivo cellular microscopic imaging methods are largely confined to animal imaging, and a major hurdle for the future is to find noninvasive methods to exploit these fluorophores in human retinal imaging.

A point spread function equal to 3 microns in all three spatial dimensions

It was recognized soon after adaptive optics was first demonstrated in the eye that its high lateral resolution would complement the ultrahigh axial resolution of OCT. By combining the two technologies in a single instrument, the point spread function can be approximately 3 microns (see Fig. 3). Miller (2011) has recently reviewed the current state of AO-OCT. Don Miller and his colleagues were the first to combine AO and an en face coherence gated camera, achieving an axial resolution of 14 microns and a lateral resolution of 3-5 microns (Miller et al., 2003). Shortly thereafter, Pablo Artal's group at the University of Murcia, Spain and Wolfgang Drexler's group at the University of Vienna collaborated to produce the first generation AO UHR OCT using time domain detection (Hermann et al., 2004a). Since then there has been a striking proliferation of AO-OCT instruments based on many different types of OCT systems including time domain en face scanning (Merino et al. 2006; Pircher, 2008), high resolution spectral domain OCT (Zhang et al., 2005; Zawadzki et al., 2005; Zhang et al., 2006; Bigelow et al., 2007; and Zawadzki et al., 2007), ultra-high spectral

NIH-PA Author Manuscript

NIH-PA Author Manuscript

NIH-PA Author Manuscript

domain OCT (Fernandez et al., 2005; Zawadzki et al., 2008; Fernandez et al., 2008; Cense et al., 2009; and Torti et al., 2009), and swept source OCT (Mujat et al., 2010).

There are a number of challenges in the successful marriage of AO and OCT. One of these is the need to correct the eye's longitudinal chromatic aberration because of the large spectral bandwidth required for high resolution OCT. The axial resolution of OCT, as mentioned earlier, is inversely proportional to the spectral bandwidth of the source. Ultrahigh resolution OCT demands sufficiently large bandwidths that chromatic aberration can significantly reduce image quality (Fernandez and Drexler, 2005; Fernandez et al., 2006). Not only does AO-OCT increase the lateral resolution up to 5 times over commercial OCT, by employing a larger pupil, it reduces the grain of speckle and increases the sensitivity of the instrument to light reflected out of the eye. AO-OCT systems have be used to image a number of retinal structures such as individual nerve bundles in the nerve fiber layer (Zawadski et al,. 2008; Cense et al., 2009; Torti et al., 2009), the smallest capillaries around the rim of the foveal avascular zone, (Hammer et al., 2008; Wang et al., 2011) as well as single cone photoreceptors (Zhang et al., 2006; Zawadski et al., 2007; Zawadski et al., 2008; Fernandez et al. 2008; Cense et al., 2009; Torti et al., 2009) It also has been deployed to study several diseases of the eye such as retinopathy of prematurity (Hammer et al., 2008) and optic neuropathies (Choi et al., 2008; 2011). Fig. 16 shows an examples of a 3-D volumetric reconstruction of the retina from an AO-OCT system

Functional changes in single cones with adaptive optics interferometry

Don Miller and his group at Indiana University have undertaken a series of very elegant experiments on single cones in the living human eye that beautifully illustrate the scientific potential of adaptive optics coupled with low coherence interferometry (Jonnal et al, 2007; 2010). While AO-OCT usually involves the use of a scanning engine and a point detector, in some cases it is possible to combine AO and low coherence interferometry to great advantage in a CCD-based flash-illuminated camera. Their flash-illuminated AO system can acquire images of cones with a high-speed CCD at rates as high as 192 Hz, ~1000 times faster than the first flood-illuminated AO ophthalmoscope he helped to build at the University of Rochester. Conveniently, most of the light reflected from cones comes from just two layers corresponding to the two ends of the cone outer segment, at the inner/outer segment junction and at the junction between the outer segment and the underlying RPE cell (see Fig. 17). Miller's instrument illuminates the cone mosaic with light of low coherence length but high enough that light reflected from these two layers within each single cone can interfere. This clever arrangement converts each cone into a living, single cell interferometer that is exquisitely sensitive to very subtle changes in optical path length within the cone. Because this interferometer, unlike most other OCT methods, has both the reference and sample beams inside the photoreceptor, it is insensitive to external vibration and motion that can plague interferometers that have separate paths for the reference and sample. Miller's group has shown for the first time that they can record an optical path length change within photoreceptors that begins within 5-10 msec of visual stimulation of a cone. Moreover, as shown in Fig. 18 they can also record the slow growth of each cone outer segment, which is only about 100 nm/hour! This process of the outer segment renewal is thought to be critical for the photoreceptor to continue to transduce light into an electrical signal and has never been resolved in vivo before. Under these specialized conditions, this instrument has the best depth resolution ever demonstrated in the eye, and can detect changes in outer segment length as small as 140 nm, more than 20 times better than the theoretical axial resolution of ultra-high resolution optical coherence tomography, and more than a 1000-fold better than the confocal scanning laser ophthalmoscope.

NIH-PA Author Manuscript

NIH-PA Author Manuscript

NIH-PA Author Manuscript

Looking forward

Aside from the satisfaction of basking in our progress, there seems to be little point in dwelling on the past unless it guides us in the future. One lesson from dwelling on the past is that the major improvements in retinal imaging technology throughout history have sprung from advances in other fields, especially optics, microscopy, and astronomy. This repeats a pattern that has pervaded the history of vision science and ophthalmology at least as early as Kepler, an astronomer who first stated unequivocally in 1604 that the retinal image is inverted. Others from the physical sciences who have made seminal contributions to vision science and ophthalmology include Helmholtz, Herschel, Maxwell, Newton, Schiener, and Young to name just a few. It is especially interesting how long it takes for significant technical advances in other fields to migrate into the eye. Confocal imaging, OCT, and adaptive optics were all introduced in other domains decades before they were applied to the eye. Part of this delay has to do with the lack of availability or high cost of the hardware required to implement new technologies; I will never forget the $1M price tag on the only deformable mirror available when I first contemplated building an adaptive optics ophthalmoscope at the University of Rochester. It also takes time to learn a new technology and to implement the modifications required to make it work in the eye. Another delay may be the result of scientific provincialism and insularity, a delay that could be reduced by increased scrutiny of the latest developments in those fields that have historically fueled ophthalmoscopy. On the bright side, if history is any guide, the next major breakthrough in retinal imaging technology was almost certainly made decades ago and is just waiting for an enterprising scientist or engineer to translate it into the eye.

The developers of new technology for retinal imaging may be unaware that they have something in common with cave divers. Both enjoy an extreme sport that is more often than not an exercise in the management of claustrophobia. The cave diver's view of his cramped world is of almost entirely impenetrable rock. The developer of retinal imaging technology is similarly boxed in by the fundamental limits of physics and biology. Both grope along, driven by the hope of discovering a previously-missed passage that, if they can just squeeze through, will open up into whole new possibilities for exploration. The history of retinal imaging would suggest, however, that fundamental limits are rarely if ever fundamental limits of the natural world. They are almost always fundamental limits of the conceptual framework we have chosen to think in. The conventional wisdom in 1990 held that axial resolution was fundamentally constrained by geometrical optics and depth of focus. But by adding the wave properties of light to the conceptual framework, practitioners of low coherence interferometry in the eye surprised everyone with a 100-fold, and now recently a 1000-fold, improvement in axial resolution over what was thought possible before.

Though it is true that the speed of light has stood its ground as a fundamental limit for a very long time, can we really say with confidence that any limits are truly impenetrable? Progress in high-resolution retinal imaging demands that we treat these limits as invitations to overcome them. It may seem that the spectral transmittance of the cornea and lens would pose a fundamental limit on noninvasive optical imaging of the retina, forever preventing us from interrogating molecules that absorb light only in spectral regions outside the ocular transmittance window. But as shown in Fig. 19, Jennifer Hunter and colleagues have recently shown that two-photon imaging can excite autofluorescent molecules in the living retina that have excitation spectra in the near UV, outside the spectral pass band of the eye's optics (Hunter et al, 2011). If this method can be made more efficient, it could open up an entirely new way to study retinal structure and function in the living eye.

Another major constraint on microscopic retinal imaging is the maximum permissible light exposure that can be delivered without damaging the eye. This constraint is especially

NIH-PA Author Manuscript

NIH-PA Author Manuscript

NIH-PA Author Manuscript

troublesome given that the typical yield in reflectance imaging is one photon back for every 10,000 that enter the pupil. The problem is compounded by the high magnification that microscopic retinal imaging demands, as well as the low efficiency of many potentially informative light-tissue interactions. But the dramatic improvements in eye tracking described earlier make it possible to maintain high spatial resolution and avoid thermal light damage by harvesting light at reduced power over longer times. Moreover, compounds have been discovered that protect the eye from photochemical light damage (eg. Maeda et al., 2006), and the application of these prior to imaging could make it possible to observe faint retinal signals that are presently invisible. In addition, we are at the beginning of a revolution in the availability of contrast enhancing fluorophores that one can direct to particular classes of retinal neurons with increasing specificity, functional imaging capabilities, and improved quantum efficiency.

The diffraction limit is another fundamental barrier that is just now coming under scrutiny in the domain of retinal microscopy (Shroff et al. 2009; 2010). Abbe (1837) showed nearly 140 years ago that the wave nature of light poses a fundamental barrier on the resolution of an optical system with a fixed numerical aperture. If the diffraction limit could be surpassed, then a new leap to smaller spatial scales in retinal imaging would be enabled, scales that in principle could be molecular. Most scientists and engineers long ago resigned themselves to the notion that the diffraction limit was so fundamental to the nature of light that it would never be surpassed in any practical imaging system. Remarkably, the field of microscopy has already seen the diffraction barrier fall, not once but many times, thanks to an array of new techniques including structured illumination (Gustafsson, 1999), stimulated emission depletion (Hell and Wichmann, 1994), and photoactivation localization microscopy (Betzig, et al., 2006). None of these methods has yet been applied successfully to retinal imaging, and certainly the challenges of doing so are formidable. But the history of the past quarter century strongly suggests that new routes around fundamental barriers will be found, allowing us to acquire ever more information from the living retina.

Acknowledgments

Thanks to Joe Carroll, Alf Dubra, Don Hood, Jennifer Hunter, Don Miller, and Austin Roorda for editorial advice in preparing this manuscript. Financial support for the research from my laboratory described in this review came from the following sources: Polgenix, Inc.; National Institute for Health Grants P30-EY001319, R01-EY004367, BRP-EY014375, T32-EY007125, R01-EY009339, R24-EY021126, R43-EY020715; This work made use of STC shared experimental facilities supported by the NSF under Agreement No. AST-9876783; Research to Prevent Blindness;

References

Arathorn DW, Yang Q, Vogel CR, Zhang Y, Tiruveedhula P, Roorda A. Retinally stabilized cone-targeted stimulus delivery. Opt Express. 2007; 15:13731–13744. [PubMed: 19550644]

Artal P, Chen L, Fernandez EJ, Singer B, Manzanera S, Williams DR. Adaptive optics for vision: the eye's adaptation to point spread function. J Refract Surg. 2003; 19(5):S585–7. [PubMed: 14518748]

Artal P, Manzanera S, Piers P, Weeber H. Visual effect of the combined correction of spherical and longitudinal chromatic aberrations. Opt Express. 2010; 18(2):1637–1648. [PubMed: 20173991]

Artal P, Navarro R. High-resolution imaging of the living human fovea: measurement of the intercenter cone distance by speckle interferometry. Optics Letters. 1989; 14:1098–1100. [PubMed: 19753067]

Atchison DA, Guo H, Charman WN, Fisher SW. Blur limits for defocus, astigmatism and trefoil. Vis Res. 2009; 49(19):2393–2403. [PubMed: 19631683]

Atchison DA, Guo H, Fisher SW. Limits of spherical blur determined with an adaptive optics mirror. Ophthalmic Physiol Opt. 2009; 29(3):300–311. [PubMed: 19422562]

NIH-PA Author Manuscript NIH-PA Author Manuscript NIH-PA Author Manuscript

Atchison DA, Guo H. Subjective blur limits for higher order aberrations. Optom Vis Sci. 2010; 87(11):E890–8. [PubMed: 20890235]

Babcock HW. The Possibility of Compensating Astronomical Seeing. PASP. 1953; 65:229–36.

Baraas RC, Carroll J, Gunther KL, Chung M, Williams DR, Foster DH, Neitz M. Adaptive optics retinal imaging reveals S-cone dystrophy in tritan color-vision deficiency. J Opt Soc Am A Opt Image Sci Vis. 2007; 24(5):1438–47. [PubMed: 17429491]

Betzig E, Patterson GH, Sougrat R, Lindwasser OW, Olenych S, et al. Imaging intracellular fluorescent proteins at nanometer resolution. Science. 2006; 313:1642–45. [PubMed: 16902090]

Bhatt SS, Rha J, Carroll J, Stepien K. Imaging photoreceptor structure in punctate inner choroidopathy using adaptive optics ophthalmoscopy and spectral domain optical coherence tomography. Invest Ophthalmol Vis Sci. 2010; 51 E-abstract 2332.

Bigelow CE, Iftimia NV, Ferguson RD, Ustun TE, Bloom B, Hammer DX. Compact multimodal adaptive-optics spectral-domain optical coherence tomography instrument for retinal imaging. J Opt Soc Am A Opt Image Sci Vis. 2007; 24(5):1327–36. [PubMed: 17429478]

Borghuis BG, Tian L, Xu Y, Nikonov SS, Vardi N, Zemelman BV, Looger LL. Imaging light responses of targeted neuron populations in the rodent retina. J Neurosci. 2011; 31(8):2855–67. [PubMed: 21414907]

Brainard DH, Roorda A, Yamauchi Y, Calderone HB, Metha A, Neitz M, Neitz J, Williams DR, Jacobs GH. Functional Consequences of the Relative Numbers of L and M Cones. J Opt Soc Am A. 2000; 17:607–614.

Brainard D, Williams DR, Hofer H. Trichromatic reconstruction from the interleaved cone mosaic: Bayesian model and the color appearance of small spots. Journal of Vision. 2008; 8(5):1–23. 15. [PubMed: 18842086]

Burns SA, Tumbar R, Elsner AE, Ferguson D, Hammer DX. Large-field-of-view, modular, stabilized, adaptive-optics-based scanning laser ophthalmoscope. J Opt Soc Am A. 2007; 24(5):1313–26.

Campbell FW, Rushton WAH. Measurement of the scotopic pigment in the living human eye. J Physiol. 1955; 130:131–147. [PubMed: 13278892]

Carroll J, Baraas RC, Wagner-Schuman M, Rha J, Siebe CA, Sloan C, Tait DM, Thompson S, Morgan JI, Neitz J, Williams DR, Foster DH, Neitz M. Cone photoreceptor mosaic disruption associated with Cys203Arg mutation in the M-cone opsin. Proc Nat'l Acad Sci USA. 2009; 106(49):20948–53. [PubMed: 19934058]

Carroll J, Choi SS, Williams DR. In vivo imaging of the photoreceptor mosaic of a rod monochromat. Vision Res. 2008; 48(26):2564–8. [PubMed: 18499214]

Carroll J, Neitz M, Hofer H, Neitz J, Williams DR. Functional photoreceptor loss revealed with adaptive optics: an alternate cause of color blindness. Proc Natl Acad Sci U S A. 2004; 101(22): 8461–6. [PubMed: 15148406]

Carroll J, Rossi EA, Porter J, Neitz J, Roorda A, Williams DR, Neitz M. Deletion of the x-linked opsin gene array locus control region (LCR) results in disruption of the cone mosaic. Vision Res. 2010; 50(19):1989–1999. [PubMed: 20638402]

Cense B, Koperda E, Brown JM, Kocaoglu OP, Gao W, Jonnal RS, Miller DT. Volumetric retinal imaging with ultrahigh-resolution spectral-domain optical coherence tomography and adaptive optics using two broadband light sources. Opt Express. 2009; 17(5):4095–111. [PubMed: 19259249]

Chen L, Artal P, Gutierrez D, Williams DR. Neural compensation for the best aberration correction. Journal of Vision. 2007; 7(10):1–9. Article 9.

Chen L, Kruger PB, Hofer H, Singer B, Williams DR. Accommodation with higher-order monochromatic aberrations corrected with adaptive optics. J Opt Soc Am A Opt Image Sci Vis. 2006; 23(1):1–8. [PubMed: 16478055]

Chen L, Singer B, Guirao A, Porter J, Williams DR. Image metrics for predicting subjective image quality. Optom Vis Sci. 2005; 82(5):358–69. [PubMed: 15894912]

Chen Y, Roorda A, Duncan JL. Advances in imaging of Stargardt disease. Adv Exp Med Biol. 2010; 664:333–40. [PubMed: 20238033]

NIH-PA Author Manuscript NIH-PA Author Manuscript NIH-PA Author Manuscript

Choi SS, Doble N, Hardy JL, Jones SM, Keltner JL, Olivier SS, Werner JS. In vivo imaging of the photoreceptor mosaic in retinal dystrophies and correlations with visual function. Invest Ophthalmol Vis Sci. 2006; 47:2080–92. [PubMed: 16639019]

Choi SS, Zawadzki RJ, Keltner JL, Werner JS. Changes in cellular structures revealed by ultra-high resolution retinal imaging in optic neuropathies. Invest Ophthalmol Vis Sci. 2008; 49(5):2103–19. [PubMed: 18436843]

Choi SS, Zawadzki RJ, Lim MC, Brandt JD, Keltner JL, Doble N, Werner JS. Evidence of outer retinal changes in glaucoma patients as revealed by ultrahigh-resolution in vivo retinal imaging. Br J Ophthalmol. 2011; 95(1):131–41. [PubMed: 20956277]

Choma M, Sarunic M, Yang C, Izatt J. Sensitivity advantage of swept source and Fourier domain optical coherence tomography. Opt Express. 2003; 11(18):2183–9. [PubMed: 19466106]

Cideciyan AV, Jacob SG. Image Analysis of the Tapetal-Like Reflex in Carriers of X-Linked Retinitis Pigmentosa. Invest Ophthalmol Vis Sci. 1994; 35:3812–3824. [PubMed: 7928178]

Cordeiro MF, Guo L, Luong V, et al. Real-time imaging of single nerve cell apoptosis in retinal neurodegeneration. Proc Natl Acad Sci USA. 2004; 101:13352–13356. [PubMed: 15340151]

Costa RA, Skaf M, Melo LA Jr, Calucci D, Cardillo JA, Castro JC, Huang D, Wojtkowski M. Retinal assessment using optical coherence tomography. Prog Retin Eye Res. 2006; 25(3):325–53. Review. [PubMed: 16716639]

Dalimier E, Dainty C. Use of a customized vision model to analyze the effects of higher-order ocular aberrations and neural filtering on contrast threshold performance. J Opt Soc Am A. 2008; 25(8): 2078–2087.

Dalimier E, Dainty C, Barbur JL. Effects of higher-order aberrations on functional vision as a function of light level. J Mod Opt. 2008; 55:791–803.

David, NJ. In Proceedings from the International Symposium on Fluorescein Angiography. Albi 1969. Vol. 1971. Basel: Karger; 1969. Infrared Absorption Fundus Angiography; p. 198-192.

de Gracia P, Dorronsoro C, Gambra E, Marin G, Hernandez M, Marcos S. Combining coma with astigmatism can improve retinal image over astigmatism alone. Vis Res. 2010; 50(19):2008–2014. [PubMed: 20659497]

Doble N, Choi SS, Codona JL, Christou J, Enoch JM, Williams DR. In vivo imaging of the human rod photoreceptor mosaic. Opt Lett. 2011; 36(1):31–3.10.1364/OL.36.000031 [PubMed: 21209677]

Dreher AW, Bille JF, Weinreb RN. Active optical depth resolution improvement of the laser tomographic scanner. Appl Opt. 1989; 28:804–808. [PubMed: 20548563]

Drexler W, Fujimoto JG. State-of-the-art retinal optical coherence tomography. Prog Retin Eye Res. 2008; 27(1):45–88. Review. [PubMed: 18036865]

Drexler W, Morgner U, Kartner FX, Pitris C, Boppart SA, Li XD, Ippen EP, Fujimoto JG. In vivo ultrahigh-resolution optical coherence tomography. Optics Letters. 1999; 24(17):1221–1223. [PubMed: 18073990]

Dubra A, Sulai Y. The reflective afocal broadband adaptive optics scanning ophthalmoscope. Biomed Opt Express. in press.

Dubra A, Sulai Y, Norris JL, Cooper RF, Dubis AM, Williams DR, Carroll J. Non-invasive in vivo imaging of the human rod photoreceptor mosaic using a confocal adaptive optics scanning ophthalmoscope. Biomed Opt Express. in press.

Elliott SL, Choi SS, Doble N, Hardy JL, Evans JW, Werner JS. Role of high-order aberrations in senescent changes in spatial vision. J Vis. 2009; 9(2):24.1–16. [PubMed: 19271934]

Fercher AF, Hitzenberger CK, Drexler W, Kamp G, Sattmann H. In vivo optical coherence tomography. Am J Ophthalmol. 1993; 116(1):113–4. [PubMed: 8328536]

Fercher AF, Hitzenberger CK, Kamp G, El-Zaiat SY. Measurement of intraocular distances by backscattering spectral interferometry. Optics Communications. 1995; 117:43–48.

Fercher AF, Mengedoht K, Werner W. Eye-length measurement by interferometry with partially coherent light. Opt Lett. 1988; 13(3):186–8. [PubMed: 19742022]

Fernandez EJ, Artal P. Study on the effects of monochromatic aberrations in the accommodation response by using adaptive optics. J Opt Soc Am A Opt Image Sci Vis. 2005; 22(9):1732–8. [PubMed: 16211799]

NIH-PA Author Manuscript

NIH-PA Author Manuscript

NIH-PA Author Manuscript

Fernandez E, Drexler W. Influence of ocular chromatic aberration and pupil size on transverse resolution in ophthalmic adaptive optics optical coherence tomography. Opt Express. 2005; 13(20):8184–97. [PubMed: 19498848]

Fernandez EJ, Hermann B, Povazay B, Unterhuber A, Sattmann H, Hofer B, Ahnelt PK, Drexler W. Ultrahigh resolution optical coherence tomography and pancorrection for cellular imaging of the living human retina. Opt Express. 2008; 16(15):11083–94. [PubMed: 18648422]

Fernandez EJ, Iglesias I, Artal P. Closed-loop adaptive optics in the human eye. Opt Lett. 2001; 26(10):746–8. [PubMed: 18040440]

Fernández EJ, Prieto PM, Artal P. Adaptive optics binocular visual simulator to study stereopsis in the presence of aberrations. J Opt Soc Am A. 2010; 27:A48–A55.

Fernandez EJ, Unterhuber A, Povazay B, Hermann B, Artal P, Drexler W. Chromatic aberration correction of the human eye for retinal imaging in the near infrared. Opt Express. 2006; 14(13): 6213–25. [PubMed: 19516794]

Fujimoto JG. Optical coherence tomography for ultrahigh resolution in vivo imaging. Nat Biotechnol. 2003; 21(11):1361–7. Review. [PubMed: 14595364]

Geng Y, Schery L, Sharma R, Dubra A, Ahmad K, Libby R, Williams DR. Optical properties of the mouse eye. Biomedical Optics Express. 2011; 2(4):717–738. [PubMed: 21483598]

Godara P, Dubis AM, Roorda A, Duncan JL, Carroll J. Adaptive optics retinal imaging: emerging clinical applications. Optom Vis Sci. 2010; 87(12):930–41. [PubMed: 21057346]

Gomez-Vieyra A, Dubra A, Malacara-Hernandez D, Williams DR. First-order design of off-axis reflective ophthalmic adaptive optics systems using afocal telescopes. Optics Express. 2009; 17(21):18906–18919. [PubMed: 20372626]

Gray DC, Merigan W, Wolfing JI, Gee BP, Porter J, Dubra A, Twietmeyer TH, Ahmad K, Tumbar R, Reinholz F, Williams DR. In vivo fluorescence imaging of primate retinal ganglion cells and retinal pigment epithelial cells. Opt Express. 2006; 14(16):7144–58. [PubMed: 19529085]

Gray DC, Wolfe R, Gee BP, Scoles D, Geng Y, Masella BD, Dubra A, Luque S, Williams DR, Merigan WH. In vivo imaging of the fine structure of rhodamine-labeled macaque retinal ganglion cells. Invest Ophthalmol Vis Sci. 2008; 49(1):467–73. [PubMed: 18172127]

Guo H, Atchison DA. Subjective blur limits for cylinder. Optometry and Vision Science. 2010; 87(8):E549–E559. [PubMed: 20562670]

Gupta P, Guo H, Atchison DA, Zele AJ. Effect of optical aberrations on the color appearance of small defocused lights. J Opt Soc Am A. 2010; 27(5):960–967.

Gustafsson MGL. Extended resolution fluorescence microscopy. Curr Opin Struct Biol. 1999; 9:627–34. [PubMed: 10508771]

Hammer DX, Ferguson RD, Bigelow CE, Iftimia NV, Ustun TE, Burns SA. Adaptive optics scanning laser ophthalmoscope for stabilized retinal imaging. Opt Express. 2006; 14(8):3354–67. [PubMed: 19516480]

Hammer DX, Iftimia NV, Ferguson RD, Bigelow CE, Ustun TE, Barnaby AM, Fulton AB. Foveal fine structure in retinopathy of prematurity: an adaptive optics Fourier domain optical coherence tomography study. Invest Ophthalmol Vis Sci. 2008; 49(5):2061–70. [PubMed: 18223243]

Hampson KM. Adaptive optics and vision. J Modern Optics. 2008; 55(21):3425–3467.

Hampson KM, Chin SS, Mallen EA. Effect of temporal location of correction of monochromatic aberrations on the dynamic accommodation response. Biomed Opt Express. 2010; 1(3):879–894. [PubMed: 21258515]

Hardy JW, Lefebvre JE, Koliopoulos CL. Real-time atmospheric compensation. J Opt Soc Am. 1977; 67:360–369.

Hecht S, Schlaer S, Pirenne MH. Energy, quanta, and vision. J Gen Physiol. 1942; 25:819–840. [PubMed: 19873316]

Hell SW, Wichmann J. Breaking the diffraction resolution limit by stimulated emission: stimulated-emission-depletion fluorescence microscopy. Opt Lett. 1994; 19:780–82. [PubMed: 19844443]

Helmholtz, HLF. Beschreibung eines Augen-Spiegels zur Untersuchung der Netzhaut im lebenden Auge [Description of an eye mirror for the investigation of the retina of the living eye]. Berlin: A Förstner'sche Verlagsbuchhandlung; 1851.

NIH-PA Author Manuscript

NIH-PA Author Manuscript

NIH-PA Author Manuscript

Hermann B, Fernandez EJ, Unterhuber A, Sattmann H, Fercher AF, Drexler W, Prieto PM, Artal P. Adaptive-optics ultrahigh-resolution optical coherence tomography. Opt Lett. 2004; 29(18):2142–4. [PubMed: 15460883]

Hofer H, Artal P, Singer B, Aragon JL, Williams DR. Dynamics of the eye's wave aberration. J Opt Soc Am A Opt Image Sci Vis. 2001a; 18(3):497–506. [PubMed: 11265680]

Hofer H, Chen L, Yoon GY, Singer B, Yamauchi Y, Williams DR. Improvement in retinal image quality with dynamic correction of the eye's aberrations. Opt Express. 2001b; 8(11):631–43. [PubMed: 19421252]

Hofer H, Carroll J, Neitz J, Neitz M, Williams DR. Organization of the human trichromatic cone mosaic. J Neurosci. 2005; 25(42):9669–79. Erratum in: J. Neurosci. 2006, 26(2), 722. [PubMed: 16237171]

Hofer H, Singer B, Williams DR. Different sensations from cones with the same photopigment. J Vis. 2005; 5(5):444–54. [PubMed: 16097875]

Hooke R. Micrographia: Some Physiological Descriptions of Minute Bodies Made by Magnifying Glasses with Observations and Inquiries Thereupon. 1664

Huang, D.; Kaiser, PK.; Lowder, CY.; Traboulsi, EI. Retinal Imaging. Elsevier, Inc.; Philadelphia: 2006.

Huang D, Swanson EA, Lin CP, Schuman JS, Stinson WG, Chang W, Hee MR, Flotte T, Gregory K, Puliafito CA. Optical coherence tomography. Science. 1991; 254(5035):1178–81. [PubMed: 1957169]

Hunter J, Masella B, Dubra A, Sharma R, Yin L, Merigan W, Palczewska G, Palczewski K, Williams DR. Images of photoreceptors in living primate eyes using adaptive optics two-photon ophthalmoscopy. Biomedical Optics Express. 2011; 2(1):139–148. [PubMed: 21326644]

Huygens C. Treatise on Light. 1678

Jackman WT, Webster JD. On photographing the retina of the living human eye. Philadelphia Photographer. 1886; 23:340–341.

Jagger WS. Visibility of photoreceptors in the intact cane toad eye. Vision Res. 1985; 25:729–31. [PubMed: 3927588]

Jonnal RS, Besecker JR, Derby JC, Kocaoglu OP, Cense B, Gao W, Wang Q, Miller DT. Imaging outer segment renewal in living human cone photoreceptors. Opt Express. 2010; 18(5):5257–70.10.1364/OE.18.005257 [PubMed: 20389538]

Jonnal RS, Rha J, Zhang Y, Cense B, Gao W, Miller DT. In vivo functional imaging of human cone photoreceptors. Opt Express. 2007; 15(4):16141–16160.

Kocaoglu OP, Lee S, Jonnal RS, Wang Q, Herde AE, Derby JC, Gao W, Miller DT. Imaging cone photoreceptors in three dimensions and in time using ultrahigh resolution optical coherence tomography with adaptive optics. Biomedical Optics Express. 2011; 2(4):748–63. [PubMed: 21483600]

Labeyrie A. Attainment of diffraction-limited resolution in large telescopes by Fourier-analyzing speckle patterns in star images. Astron Astrophys. 1970; 6:85–87.

Land MF, Snyder AW. Cone mosaic observed directly through natural pupil of live vertebrate. Vision Res. 1985; 25:1519–23. [PubMed: 4090286]

Leung CK, Lindsey JD, Growston JG, Lijia C, Chiang S, Weinreb RN. Longitudinal profile of retinal ganglion cell damage after optic nerve crush with blue-light confocal scanning laser ophthalmoscopy. Invest Ophthalmol Vis Sci. 2008; 49:4898–4902. [PubMed: 18441315]

Li J, Xiong Y, Wang N, Li S, Dai Y, Xue L, Zhao H, Jiang W, Zhang Y. Effects of spherical aberration on visual acuity at different contrasts. J Cataract Refract Surg. 2009; 35(8):1389–1395. [PubMed: 19631126]

Li S, Xiong Y, Li J, Wang N, Dai Y, Xue L, Zhao H, Jiang W, Zhang Y, He JC. Effects of monochromatic aberration on visual acuity using adaptive optics. Optom Vis Sci. 2009; 86(7): 868–874. [PubMed: 19521271]

Liang J, Grimm B, Goelz S, Bille JF. Objective measurement of wave aberrations of the human eye with the use of a Hartmann–Shack wavefront sensor. J Opt Soc Am A. 1994; 11:1949–1957.

Liang J, Williams DR. Aberrations and retinal image quality of the normal human eye. J Opt Soc Am A. 1997; 14:2873–2883.

NIH-PA Author Manuscript

NIH-PA Author Manuscript

NIH-PA Author Manuscript

Liang J, Williams DR, Miller DT. Supernormal vision and high-resolution retinal imaging through adaptive optics. J Opt Soc Am A Opt Image Sci Vis. 1997; 14(11):2884–92. [PubMed: 9379246]

Lundstrom L, Manzanera S, Prieto PM, Ayala DB, Gorceix N, Gustafsson J, Unsbo P, Artal P. Effect of optical correction and remaining aberrations on peripheral resolution acuity in the human eye. Opt Express. 2007; 15(20):12654–61. [PubMed: 19550533]

MacLean AL, Maumenee AE. Hemangioma of the choroid. Am I Ophthalmol. 1960; 50(1):3–11.

Maeda A, Maeda T, Golczak M, Imanishi Y, Leahy P, Kubota R, Pasczewski K. Effects of potent inhibitors of the retinoid cycle on visual function and photoreceptor protection from light damage in mice. Mol Pharmacol. 2006; 70(4):1220–9. [PubMed: 16837623]

Marcos S, Sawides L, Gambra E, Dorronsoro C. Influence of adaptive- optics ocular aberration correction on visual acuity at different luminances and contrast polarities. J Vis. 2008; 8(13):1–12.

Martin JA, Roorda A. Direct and noninvasive assessment of parafoveal capillary leukocyte velocity. Ophthalmology. 2005; 112(12):2219–24. [PubMed: 16257054]

Martin JA, Roorda A. Pulsatility of parafoveal capillary leukocytes. Exp Eye Res. 2009; 88(3):356–60. [PubMed: 18708051]

Masters, BR.; Thompson, BJ. Selected Papers on Optical Low-Coherence Reflectometry & Tomography. Vol. MS 165. Bellingham, Washington: 2001. SPIE Milestone Series

McAllister JT, Dubis AM, Tait DM, Ostler S, Rha J, Stepien KE, Summers CG, Carroll J. Arrested development: high-resolution imaging of foveal morphology in albinism. Vis Res. 2010; 50:810–7. [PubMed: 20149815]

Merino D, Dainty C, Bradu A, Podoleanu AG. Adaptive optics enhanced simultaneous en-face optical coherence tomography and scanning laser ophthalmoscopy. Opt Express. 2006; 14(8):3345–53. [PubMed: 19516479]

Miller DT, Kocaoglu OP, Wang Q, Lee S. Adaptive optics and the eye (super resolution OCT). Eye. 2011; 25(3):321–330. [PubMed: 21390066]

Miller DT, Qu J, Jonnal RS, Thorn K. Coherence Gating and Adaptive Optics in the Eye. Proc SPIE. 2003; 4956:65–72.

Miller, DT.; Roorda, A. Adaptive optics in retinal microscopy and vision. In: Bass, M.; Decusatis, C.; Enoch, JM.; Lakshminarayanan, V.; Li, G.; Macdonald, C.; Mahajan, VN.; Van Stryland, E., editors. Handbook of Optics. 3rd. Vol. III. Vision and Vision Optics; McGraw Hill, New York: 2009. Ch. 17

Miller D, Williams DR, Morris GM, Liang J. Images of cone photoreceptors in the living human eye. Vision Res. 1996; 36:1067–1079. [PubMed: 8762712]

Minsky, M. US Patent #3,013,467. 1957. p. 128-138.described in Scanning, 10, 1988

Morgan JIW, Dubra A, Wolfe R, Merigan WH, Williams DR. In vivo autofluorescence imaging of the human and macaque retinal pigment epithelial cell mosaic. IOVS. 2009; 50(3):1350–1359.

Mujat M, Ferguson RD, Patel AH, Iftimia N, Lue N, Hammer DX. High resolution multimodal clinical ophthalmic imaging system. Opt Express. 2010; 18(11):11607–21.10.1364/OE.18.011607 [PubMed: 20589021]

Neitz J, Carroll J, Yamauchi Y, Neitz M, Williams DR. Color Perception is Mediated by a Plastic Neural Mechanism that Remains Adjustable in Adults. Neuron. 2002; 35:783–792. [PubMed: 12194876]

Novotny R, Alvis DL. A Method of Photographing Fluorescence in Circulating Blood in the Human Retina. Circulation. 1961; 24:82–86. [PubMed: 13729802]

Ogle KN, Rucker CW. Fundus photographs in color using a high speed flash tube in the Zeiss retinal camera. AMA Arch Ophthal. 1953; 49:435–438. [PubMed: 13030023]

Pacques M, Simonuti M, Roux MJ, Picaud S, Levavasseiu E, Bellman C, Sahel JA. High resolution fundus imaging by confocal scanning laser ophthalmoscopy in the mouse. Vision Res. 2006; 46:1336–1345. [PubMed: 16289196]

Perez GM, Manzanera S, Artal P. Impact of scattering and spherical aberration in contrast sensitivity. JVis. 2009; 9(3):19-1–10. [PubMed: 19757958]

Pircher M, Baumann B, Götzinger E, Hitzenberger CK. Retinal cone mosaic imaged with transverse scanning optical coherence tomography. Opt Lett. 2006; 31(12):1821–3. [PubMed: 16729082]

NIH-PA Author Manuscript

NIH-PA Author Manuscript

NIH-PA Author Manuscript

Pircher M, Zawadzki RJ, Evans JW, Werner JS, Hitzenberger CK. Simultaneous imaging of human cone mosaic with adaptive optics enhanced scanning laser ophthalmoscopy and high-speed transversal scanning optical coherence tomography. Opt Lett. 2008; 33(1):22–4. [PubMed: 18157245]

Podoleanu AG. Optical coherence tomography. Br J Radiol. 2005; 78(935):976–88. Review. [PubMed: 16249597]

Podoleanu AG, Rosen RB. Combinations of techniques in imaging the retina with high resolution. Prog Retin Eye Res. 2008; 27(4):464–99. Review. [PubMed: 18495519]

Porter, J.; Queener, H.; Lin, J.; Thorn, K.; Awwal, A. Adaptive Optics for Vision Science. John Wiley & Sons, Inc.; Hoboken, New Jersey: 2006.

Putnam NM, Hofer HJ, Doble N, Chen L, Carroll J, Williams DR. The locus of fixation and the foveal cone mosaic. J Vis. 2005; 5(7):632–9. [PubMed: 16231998]

Raghunandan A, Frasier J, Poonja S, Roorda A, Stevenson SB. Psychophysical measurements of referenced and unreferenced motion processing using high-resolution retinal imaging. J Vis. 2008; 8(14):14.1–11. [PubMed: 19146315]

Rocha KM, Vabre L, Chateau N, Krueger RR. Enhanced visual acuity and image perception following correction of highly aberrated eyes using an adaptive optics visual simulator. J Refract Surg. 2010; 26(1):52–56. [PubMed: 20199013]

Rocha KM, Vabre L, Harms F, Chateau N, Krueger RR. Effects of Zernike wavefront aberrations on visual acuity measured using electromagnetic adaptive optics technology. J Refract Surg. 2007; 23(9):953–959. [PubMed: 18041253]

Rouger H, Benard Y, Legras R. Effect of monochromatic induced aberrations on visual performance measured by adaptive optics technology. J Refract Surg. 2009; 11:1–10.

Roorda A. Applications of adaptive optics scanning laser ophthalmoscopy. Optom Vis Sci. 2010; 87(4):260–8. Review. [PubMed: 20160657]

Roorda A, Metha A, Lennie P, Williams DR. Packing arrangement of the three cone classes in the primate retina. Vision Research. 2001; 41(12):1291–1306. [PubMed: 11322974]

Roorda A, Romero-Borja F, Donnelly IW, Queener H, Hebert T, Campbell M. Adaptive optics scanning laser ophthalmoscopy. Opt Express. 2002; 10(9):405–12. [PubMed: 19436374]

Roorda A, Williams DR. The arrangement of the three cone classes in the living human eye. Nature. 1999; 397(6719):520–2. [PubMed: 10028967]

Roorda A, Zhang Y, Duncan JL. High-resolution in vivo imaging of the RPE mosaic in eyes with retinal disease. Invest Ophthalmol Vis Sci. 2007; 48(5):2297–303. [PubMed: 17460294]

Rossi EA, Chung M, Dubra A, Hunter JJ, Merigan WH, Williams DR. Imaging retinal mosaics in the living eye. Eye. 2011:1–8. [PubMed: 21178995]

Rossi EA, Roorda A. Is visual resolution after adaptive optics correction susceptible to perceptual learning? J Vis. 2010; 10(12):11. [PubMed: 21047743]

Rossi EA, Weiser P, Tarrant J, Roorda A. Visual performance in emmetropia and low myopia after correction of high-order aberrations. J Vis. 2007; 7(8):14. [PubMed: 17685821]

Sabesan R, Yoon G. Neural compensation for long-term asymmetric optical blur to improve visual performance in keratoconic eyes. Invest Ophthalmol Vis Sci. 2010; 51(7):3835–9. [PubMed: 20130284]

Sawides L, Gambra E, Pascual D, Dorronsoro C, Marcos S. Visual performance with real-life tasks under adaptive-optics ocular aberration correction. J Vis. 2010; 10(5):19.10.1167/10.5.19 [PubMed: 20616133]

Schuman, JS.; Puliafito, CA.; Fujimoto, JG. Optical Coherence Tomography of Ocular Diseases. 2nd. Slack Inc.; Thorofare, NJ: 2004. spelled “Schulman” in your doc

Seeliger MW, Beck SC, Pereyra-Munoz N, Dangel S, Tsai JY, Luhmann UF, van de Pavert SA, Wijnholds J, Samardzija M, Wenzel A, Zrenner E, Narfstrom K, Fahl E, Tanimoto N, Acar N, Tonagel F. In vivo confocal imaging of the retina in animal models using scanning laser ophthalmoscopy. Vis Res. 2005; 45:3512–3519. [PubMed: 16188288]

Shroff S, Fienup JR, Williams DR. Phase-shift estimation in sinusoidally illuminated images for lateral superresolution. J Opt Soc Am A Opt Image Sci Vis. 2009; 26(2):413–424. [PubMed: 19183696]

NIH-PA Author Manuscript NIH-PA Author Manuscript NIH-PA Author Manuscript

Shroff S, Fienup JR, Williams DR. Lateral superresolution using a posteriori phase shift estimation for a moving object – experimental results. J Opt Soc Am A Opt Image Sci Vis. 2010; 27(8):1770–82. [PubMed: 20686581]

Sincich LC, Zhang Y, Tiruveedhula P, Horton JC, Roorda A. Resolving single cone inputs to visual receptive fields. Nat Neurosci. 2009; 12(8):967–9. [PubMed: 19561602]

Smirnov MS. Measurement of the wave aberration of the human eye. Biophysics. 1961; 6:687–703.

Stevenson, SB.; Roorda, A. Correcting for miniature eye movements in high resolution scanning laser ophthalmoscopy. In: Manns, F.; Soderberg, P.; Ho, A., editors. Ophthalmic Technologies XI. Bellingham, WA: SPIE; 2005. p. 45-151.

Talcott KE, Ratnam K, Sundquist SM, Lucero AS, Lujan BJ, Tao W, Porco TC, Roorda A, Duncan JL. Longitudinal study of cone photoreceptors during retinal degeneration and in response to ciliary neurotrophic factor treatment. Invest Ophthalmol Vis Sci. 2011; 52(5):2219–26. [PubMed: 21087953]

Talcott KE, Sundquist S, Solovyev A, Lujan BJ, Tao W, Roorda A, Duncan JL. High-resolution in-vivo imaging of cone photoreceptors in eyes treated with sustained-release ciliary neurotrophic factor in patients with retinitis pigmentosa. Invest Ophthalmol Vis Sci. 2010; 51 E-abstract 1385.

Tam J, Martin JA, Roorda A. Noninvasive visualization and analysis of parafoveal capillaries in humans. Invest Ophthalmol Vis Sci. 2010; 51:1691–1698. [PubMed: 19907024]

Tam J, Tiruveedhula P, Roorda A. Characterization of single-file flow through human retinal parafoveal capillaries using an adaptive optics scanning laser ophthalmoscope. Biomed Opt Express. 2011; 2(4):781–93. [PubMed: 21483603]

Torti C, Povazay B, Hofer B, Unterhuber A, Carroll J, Ahnelt PK, Drexler W. Adaptive optics optical coherence tomography at 120,000 depth scans/s for non-invasive cellular phenotyping of the living human retina. Opt Express. 2009; 17(22):19382–400.10.1364/OE.17.019382 [PubMed: 19997159]

Vogel CR, Arathorn DW, Roorda A, Parker A. Retinal motion estimation and image dewarping in adaptive optics scanning laser ophthalmoscopy. Opt Express. 2006; 14:487–497. [PubMed: 19503363]

Vohnsen B, Iglesias I, Artal P. High-resolution imaging of the in-vivo human eye retina. Opt Lett. 2004; 29(9):968–70. [PubMed: 15143643]

von Ruckmann A, Fitzke FW, Bird AC. Distribution of fundus autofluorescence with a scanning laser ophthalmoscope. Br J Ophthalmol. 1995; 79:407–412. [PubMed: 7612549]

Wade AR, Fitzke FW. In-vivo imaging of the human cone photoreceptor mosaicusing a confocal LSO. Lasers Light Ophthalmol. 1998; 8:129–36.

Wagner-Schuman M, Neitz J, Rha J, Williams DR, Neitz M, Carroll J. Color-deficient cone mosaics associated with Xq28 opsin mutations: a stop codon versus gene deletions. Vision Res. 2010; 50(23):2396–402. [PubMed: 20854834]

Walsh G, Charman WN, Howland HC. Objective technique for the determination of monochromatic aberrations of the human eye. J Opt Soc Am A. 1984; 1:987–992. [PubMed: 6481506]

Walsh MK, Quigley HA. In vivo time-lapse fluorescence imaging of individual retinal ganglion cells in mice. J Neurosci Methods. 2008; 169:214–221. [PubMed: 18199485]

Wang Q, Kocaoglu OP, Cense B, Bruestle J, Jonnal RS, Gao W, Miller DT. Imaging retinal capillaries using ultrahigh-resolution optical coherence tomography and adaptive optics. Invest Ophthalmol Vis Sci. 2011 in press.

Webb RH, Hughes GW, Delori FC. Confocal scanning laser ophthalmoscope. Appl Opt. 1987; 26(8): 1492–9.10.1364/AO.26.001492 [PubMed: 20454349]

Webb RH, Hughes GW, Pomerantzeff O. Flying spot TV ophthalmoscope. Appl Opt. 1980; 19:2991–2997. [PubMed: 20234539]

Werner JS, Keltner JL, Zawadzki RJ, Choi SS. Outer retinal abnormalities associated with inner retinal pathology in nonglaucomatous and glaucomatous optic neuropathies. Eye. 2011; 25:279–289. [PubMed: 21293495]

Williams DR. Visibility of interference fringes near the resolution limit. J Opt Soc Am A. 1985; 2:1087–1093. [PubMed: 4020506]

NIH-PA Author Manuscript NIH-PA Author Manuscript NIH-PA Author Manuscript

Williams DR. Topography of the foveal cone mosaic in the living human eye. Vision Res. 1988; 28:433–454. [PubMed: 3188406]

Williams, DR.; Hofer, H. Formation and acquisition of the retinal image. In: Chalupa, LM.; Werner, JS., editors. The Visual Neurosciences. MIT Press; Cambridge, MA: 2003. p. 795-810.

Williams DR, MacLeod DIA, Hayhoe MM. Punctate sensitivity of the blue sensitive mechanism. Vision Res. 1981; 21:1357–1376. [PubMed: 7314519]

Williams D, Yoon GY, Porter J, Guirao A, Hofer H, Cox I. Visual benefit of correcting higher order aberrations of the eye. J Refract Surg. 2000; 16(5):S554–S559. [PubMed: 11019871]

Wilt B, Burns L, Ho E, Ghosh K, Mukamel E, Schnitzer M. Advances in Light Microscopy for Neuroscience. Annu Rev Neurosci. 2009; 32:435–506. [PubMed: 19555292]

Wojtkowski M. High-speed optical coherence tomography: basics and applications. Appl Opt. 2010; 49(16):D30–61. Review. 10.1364/AO.49.000D30 [PubMed: 20517358]

Wojtkowski M, Kowalczyk A, Leitgeb R, Fercher AF. Full range complex spectral optical coherence tomography technique in eye imaging. Opt Lett. 2002a; 27(16):1415–7. [PubMed: 18026464]

Wojtkowski M, Leitgeb R, Kowalczyk A, Bajraszewski T, Fercher AF. In vivo human retinal imaging by Fourier domain optical coherence tomography. J Biomed Opt. 2002b; 7(3):457–63. [PubMed: 12175297]

Wolfing JI, Chung M, Carroll J, Roorda A, Williams DR. High-resolution retinal imaging of cone-rod dystrophy. Ophthalmology. 2006; 113:1019.e1. [PubMed: 16650474]

Yang Q, Arathorn DW, Tiruveedhula P, Vogel CR, Roorda A. Design of an integrated hardware interface for AOSLO image capture and cone-targeted stimulus delivery. Opt Express. 2010; 18:17841–17858. [PubMed: 20721171]

Yin, L.; Williams, DR. Adaptive Optics. In: Behearse, JC.; Bok, D., editors. The Retina and its Disorders. Academic Press; 2011.

Yoon GY, Williams DR. Visual performance after correcting the monochromatic and chromatic aberrations of the eye. J Opt Soc Am A Opt Image Sci Vis. 2002; 19(2):266–75. [PubMed: 11822589]

Yoon MK, Roorda A, Zhang Y, Nakanishi C, Wong LJ, Zhang Q, Gillum L, Green A, Duncan JL. Adaptive optics scanning laser ophthalmoscopy images in a family with the mitochondrial DNA T8993C mutation. Invest Ophthalmol Vis Sci. 2009; 50:1838–47. [PubMed: 18997096]

Young T. On the mechanism of the eye. Philosophical Transactions of the Royal Society of London. 1801; 91(Part I):23–88. + plates.

Young T. Experimental Demonstration of the General Law of the Interference of Light. Philos Trans R Soc London. 1804; 94:1–16.

Zawadzki RJ, Cense B, Zhang Y, Choi SS, Miller DT, Werner JS. Ultrahigh-resolution optical coherence tomography with monochromatic and chromatic aberration correction. Opt Express. 2008; 16(11):8126–43. [PubMed: 18545525]

Zawadzki RJ, Choi SS, Jones SM, Oliver SS, Werner JS. Adaptive optics-optical coherence tomography: optimizing visualization of microscopic retinal structures in three dimensions. J Opt Soc Am A Opt Image Sci Vis. 2007; 24(5):1373–83. [PubMed: 17429483]

Zawadzki RJ, Jones SM, Olivier SS, Zhao M, Bower BA, Izatt JA, Choi S, Laut S, Werner JS. Adaptive-optics optical coherence tomography for high-resolution and high-speed 3D retinal in vivo imaging. Opt Express. 2005; 13(21):8532–8546. [PubMed: 19096728]

Zhang Y, Cense B, Rha J, Jonnal RS, Gao W, Zawadzki RJ, Werner JS, Jones S, Olivier S, Miller DT. High-speed volumetric imaging of cone photoreceptors with adaptive optics spectral-domain optical coherence tomography. Opt Express. 2006; 14(10):4380–94. [PubMed: 19096730]

Zhang Y, Rha J, Jonnal RS, Miller DT. AO parallel spectral domain optical coherence tomography for imaging the living retina. Opt Express. 2005; 13:4792–4811. [PubMed: 19495398]

Zhong Z, Petrig BL, Qi X, Burns SA. In vivo measurement of erythrocyte velocity and retinal blood flow using adaptive optics scanning laser ophthalmoscopy. Opt Express. 2008; 16(17):12746–56. [PubMed: 18711513]

Zhong Z, Song H, Chui TY, Petrig BL, Burns SA. Non-invasive measurements and analysis of blood velocity profiles in human retinal vessels. Invest Ophthalmol Vis Sci. 2011 in press.

NIH-PA Author Manuscript

NIH-PA Author Manuscript

NIH-PA Author Manuscript

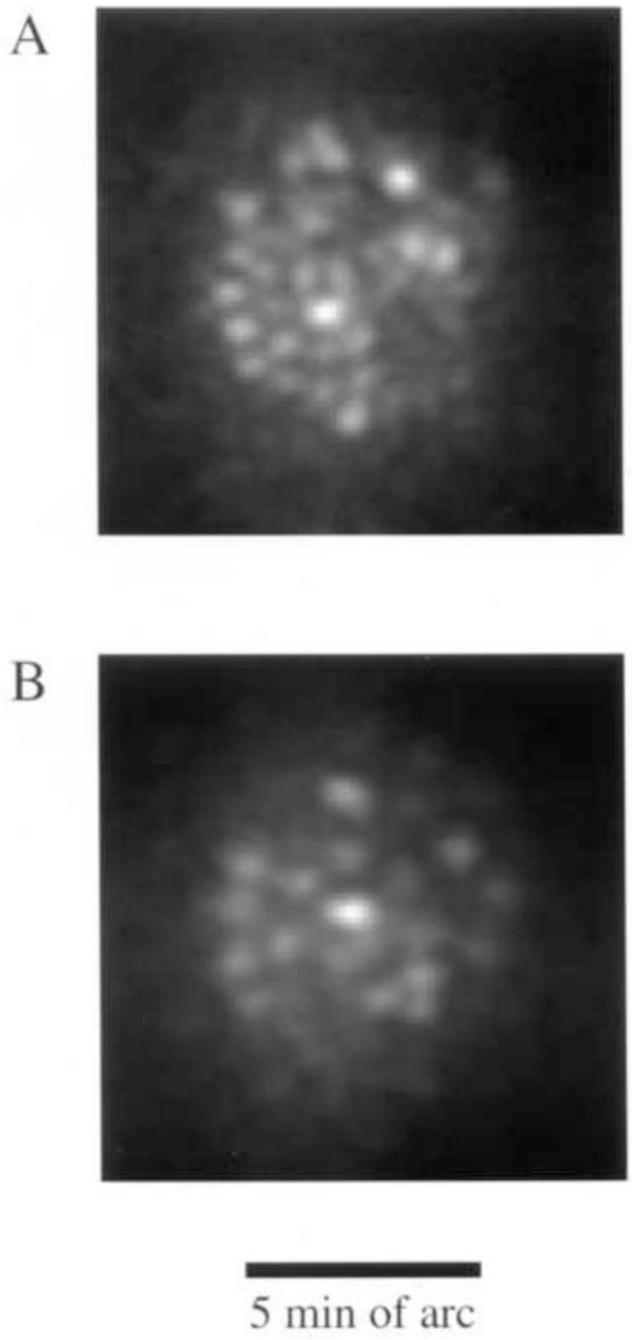

Fig. 1.

Some of the first images taken of the human photoreceptor mosaic in the human eye with a high magnification fundus camera and the method developed by Miller et al. (1996). A. Image obtained at 0.5 deg from the foveal center. B) Image obtained at 2.5 deg from the foveal center.

NIH-PA Author Manuscript

NIH-PA Author Manuscript

NIH-PA Author Manuscript

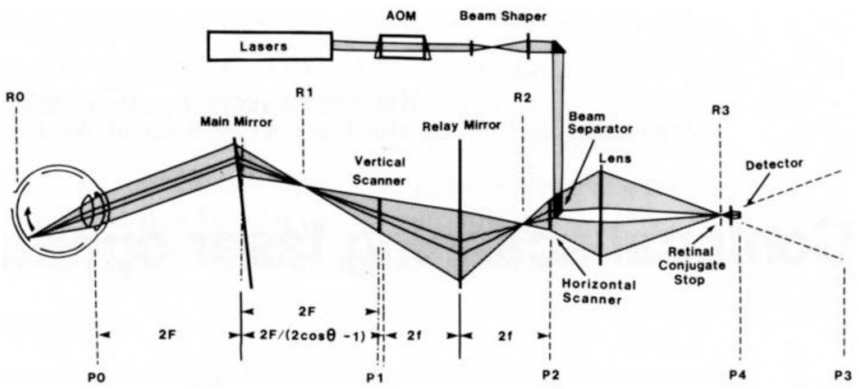

Fig. 2.

Optical layout of the first confocal SLO. The light path is shown at one instant in time. Mirrors are shown as transmissive for simplicity. Pupil conjugate planes are labeled with P_n. P_3 is a virtual image of the pupil, converted to a real image at P_4 by a microscope objective. Retinal conjugate planes are labeled with R_n. R_3 corresponds to the confocal pinhole just in front of the light detector. From: Webb, R.H., Hughes, G.W., Delori, F.C., (1987).

NIH-PA Author Manuscript

NIH-PA Author Manuscript

NIH-PA Author Manuscript

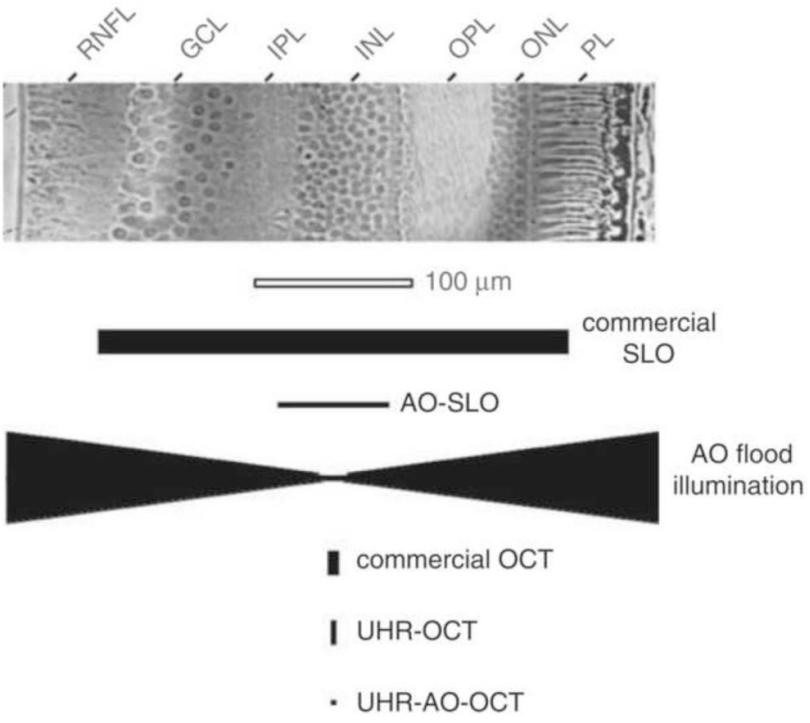

Fig. 3.

Comparison of (top) cell size in a histological cross section of the human retina with (bottom) the resolving capability of the major types of retinal imaging modalities with and without AO. The vertical and horizontal dimensions of the solid black symbols denote, respectively, the lateral and axial resolution of the instruments. Examples shown include the commercial confocal scanning laser ophthalmoscope (SLO), adaptive optics confocal scanning laser ophthalmoscope (AOSLO), adaptive optics flood illumination, commercial OCT, ultrahigh-resolution OCT (UHR–OCT), and ultrahigh-resolution OCT with adaptive optics (UHR–AO– OCT). GCL, ganglion cell layer; IPL, inner plexiform layer; INL, inner nuclear layer; OPL, outer plexiform layer; ONL, outer nuclear layer; PL, photoreceptor layer; RNFL, retinal nerve fiber layer. From Miller (2011).

NIH-PA Author Manuscript

NIH-PA Author Manuscript

NIH-PA Author Manuscript

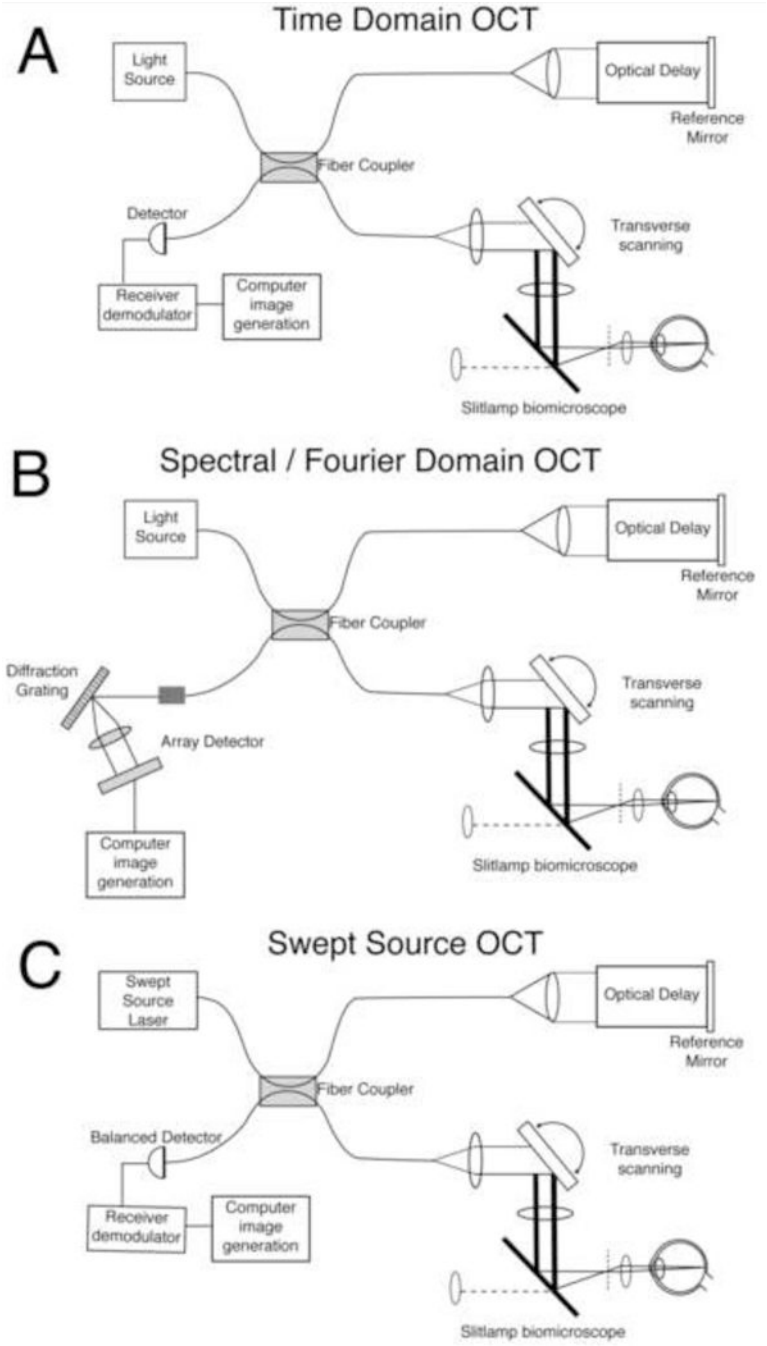

Fig. 4.

Three methods that use low coherence interferometry to acquire high resolution depth information from the retina. A) Time domain OCT B) Spectral or Fourier Domain OCT. C) Swept Source OCT. See text for details. Adapted from Fujimoto (2003).

NIH-PA Author Manuscript

NIH-PA Author Manuscript

NIH-PA Author Manuscript

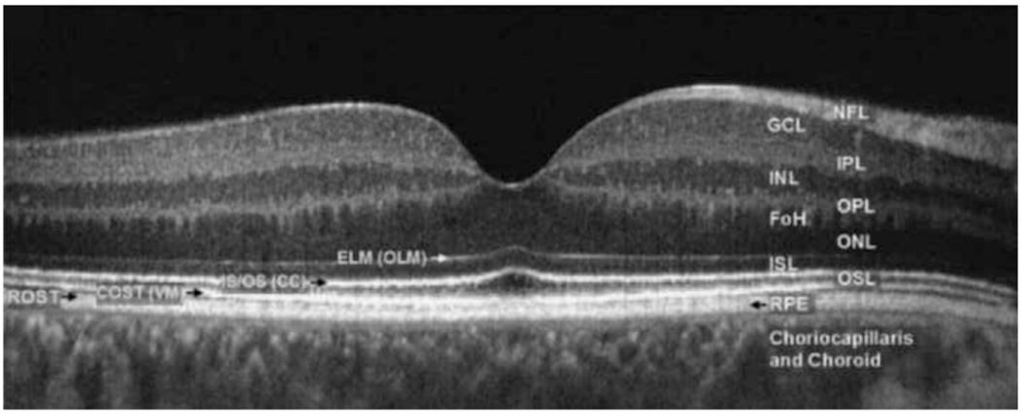

Fig. 5.

Fourier-domain optical coherence tomography (FD-OCT) B-scan of the fovea from a normal 34-year-old volunteer acquired with a FD-OCT instrument scanning 5mm laterally. The instrument was built by Jack Werner's group at UC, Davis. Abbreviations: FoH, fibers of Henle; GCL, ganglion cell layer; INL, inner nuclear layer; IPL, inner plexiform layer; ISL, inner segment layer; NFL, nerve fiber layer; ONL, outer nuclear layer; OPL, outer plexiform layer; OSL, outer segment layer; RPE, retinal pigment epithelium, choriocapillaris and choroid. The outer limiting membrane (OLM; sometimes called external limiting membrane (ELM)), connecting cilia (CC; sometimes called inner/outer segment junction), Verhoeff's membrane (VM; sometimes called cone photoreceptor outer segment tips (COST)) and rod photoreceptor outer segment tips (ROST) may also be seen. ROST and RPE appear as one layer in the fovea but are visible as separate layers in the periphery. From Werner et al. (2011).

NIH-PA Author Manuscript

NIH-PA Author Manuscript

NIH-PA Author Manuscript

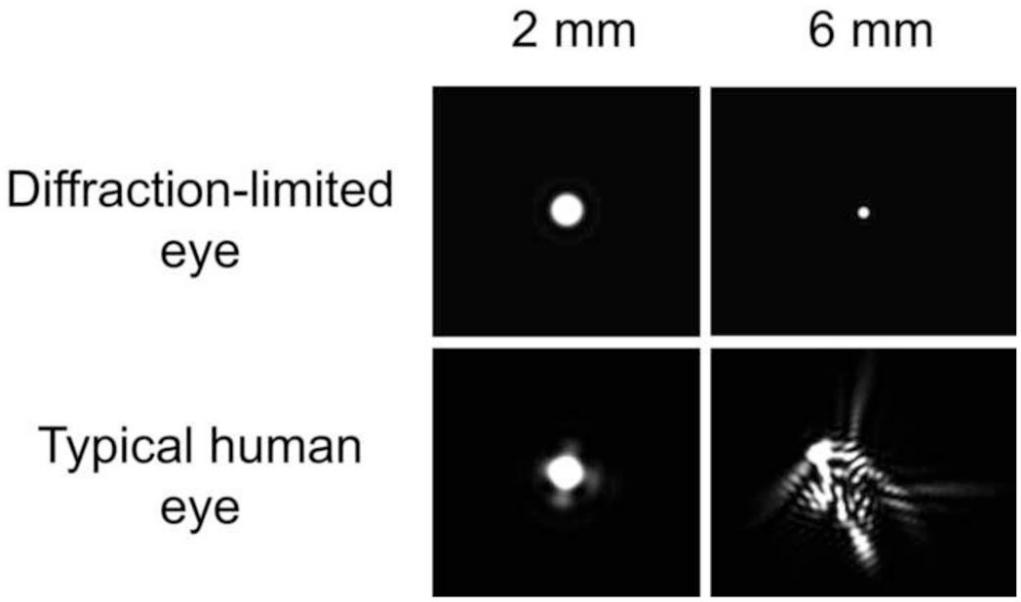

Fig. 6.
The point spread function (PSF) for a diffraction-limited eye and a normal eye at two different pupil diameters. The PSF corresponds to the light distribution on the retina produced by a point source of light infinitely distant from the eye. For the hypothetical diffraction-limited eye, the PSF diameter decreases in inverse proportion to the pupil diameter such that large pupils produce the best image quality. However, in the typical human eye, aberrations increase with increasing pupil size, eliminating the benefit of escaping diffraction at the largest pupils. The goal of AO is to correct the aberrations to produce the PSF of a diffraction-limited eye with a large pupil. (From Yin and Williams, 2010)

NIH-PA Author Manuscript

NIH-PA Author Manuscript

NIH-PA Author Manuscript

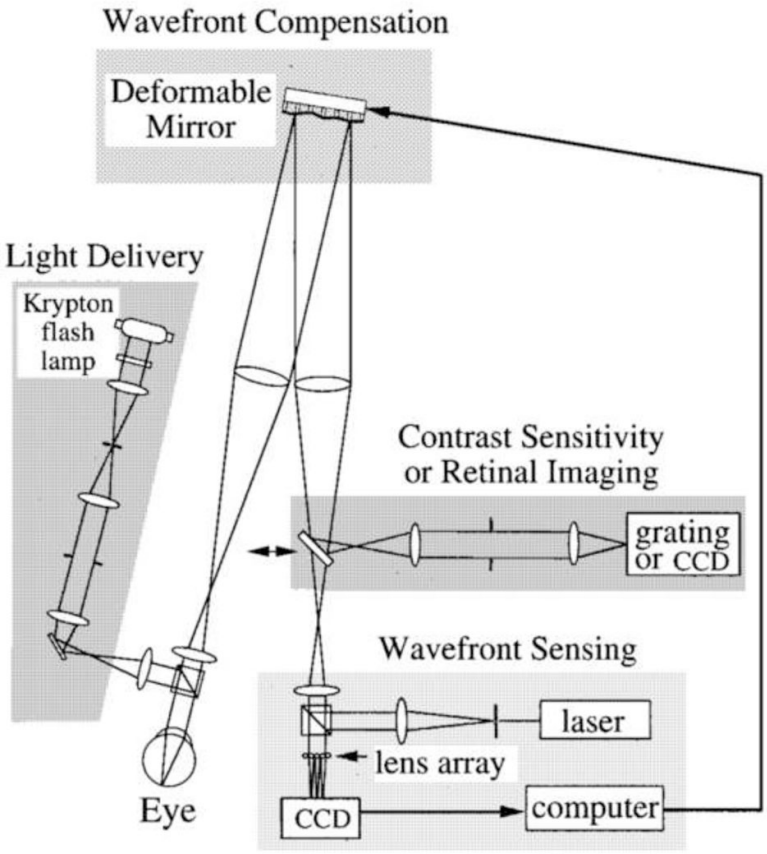

Fig. 7.

Optical layout of the first adaptive optics fundus camera that could correct higher order aberrations of the human eye. *Wave-front sensing and adaptive compensation*. The eye focused a collimated laser beam onto the retina. The light reflected from the retina formed an aberrated wave front at the pupil. The distorted wave front was measured by a Hartmann–Shack wave-front sensor. A deformable mirror, conjugate with the pupil, compensated for the eye's wave aberration. After compensation was achieved, psychophysical or retinal imaging experiments could be performed with a 6-mm pupil. *Retinal imaging*. A krypton flash lamp delivered a 4-ms flash, illuminating a retinal disk 1 deg in diameter. A scientific-grade CCD acquired images of the retina. From Liang et al. (1997).

NIH-PA Author Manuscript

NIH-PA Author Manuscript

NIH-PA Author Manuscript

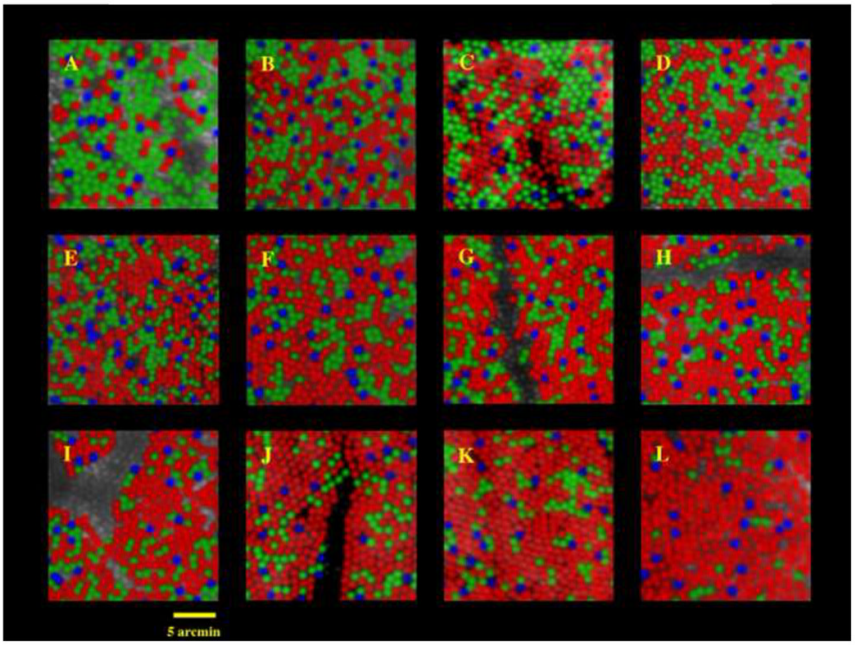

Fig. 8.

Images of the cone mosaics of 10 subjects with normal color vision, obtained with the combined methods of adaptive optics imaging and retinal densitometry. The images are false colored so that blue, green, and red are used to represent the S, M, and L cones respectively. (The true colors of these cones are yellow, purple, and bluish-purple). The mosaics illustrate the enormous variability in L/M cone ratio. The L/M cone ratios are A,0.37, B, 1.11, C, 1.14, D, 1.24, E, 1.77, F, 1.88, G, 2.32, H, 2.36, I, 2.46, J, 3.67, K, 3.90, L, 16.54. The proportion of S cones is relatively constant across eyes, ranging from 3.9 to 6.6% of the total population. Images were taken either 1 or 1.25 deg from the foveal center. For two of the 10 subjects, two different retinal locations are shown. Panels D and E show images from nasal and temporal retinas respectively for one subject; J and K show images from nasal and temporal retinas for another subject. Images C, J, and K are from Roorda and Williams (1999). All other images are from Hofer et al. (2004). From Williams and Hofer, H. (2003).

NIH-PA Author Manuscript

NIH-PA Author Manuscript

NIH-PA Author Manuscript

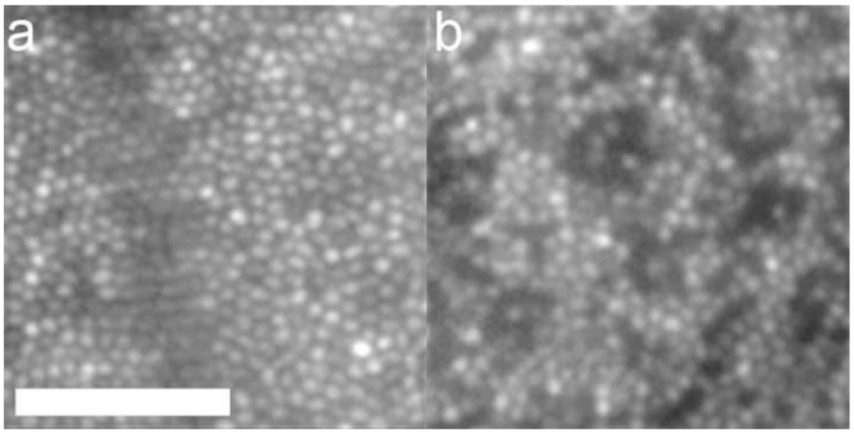

Fig. 9.

AO reveals cone mosaics in two kinds of color blindness. (a) Dichromat with cone mosaic indistinguishable from a normal trichromat. (b) Dichromat with M pigment mutation showing dark regions where cones may be damaged or lost; despite the disruption in the cone mosaic this person has excellent spatial vision. Scale is identical for each panel; scale bar is 50 microns. From Carroll et al. (2004).

NIH-PA Author Manuscript

NIH-PA Author Manuscript

NIH-PA Author Manuscript

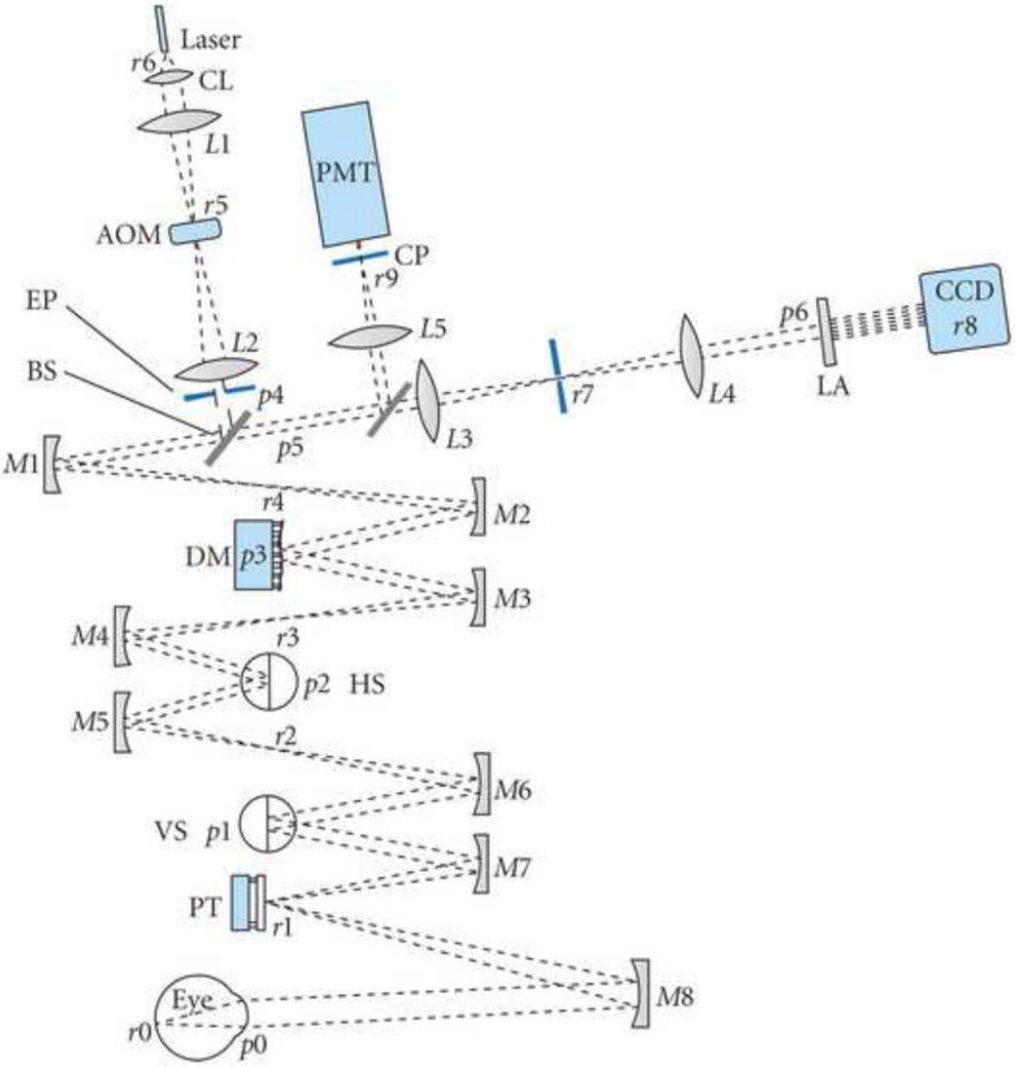

Fig. 10.

Schematic of an adaptive optics scanning laser ophthalmoscope invented by Austin Roorda. Key: CL—collimating lens; AOM—acousto-optic modulator; EP—entrance pupil; BS1—beamsplitter 1; DM—deformable mirror; HS—horizontal scanning mirror; VS—vertical scanning mirror; PT—pupil tracking mirror; LA—lenslet array; CP—confocal pinhole; PMT—photomultiplier tube. Pupil and retinal conjugates are labeled *p* and *r*, respectively. Mirrors and lenses are labeled M# and L# along the optical path. Telescope lens/mirror-pairs for relaying the pupil through the path are *L1–L2, L3–L4, M1–M2, M3–M4, M5–M6, and M7–M8*. From Miller and Roorda (2009).

NIH-PA Author Manuscript

NIH-PA Author Manuscript

NIH-PA Author Manuscript

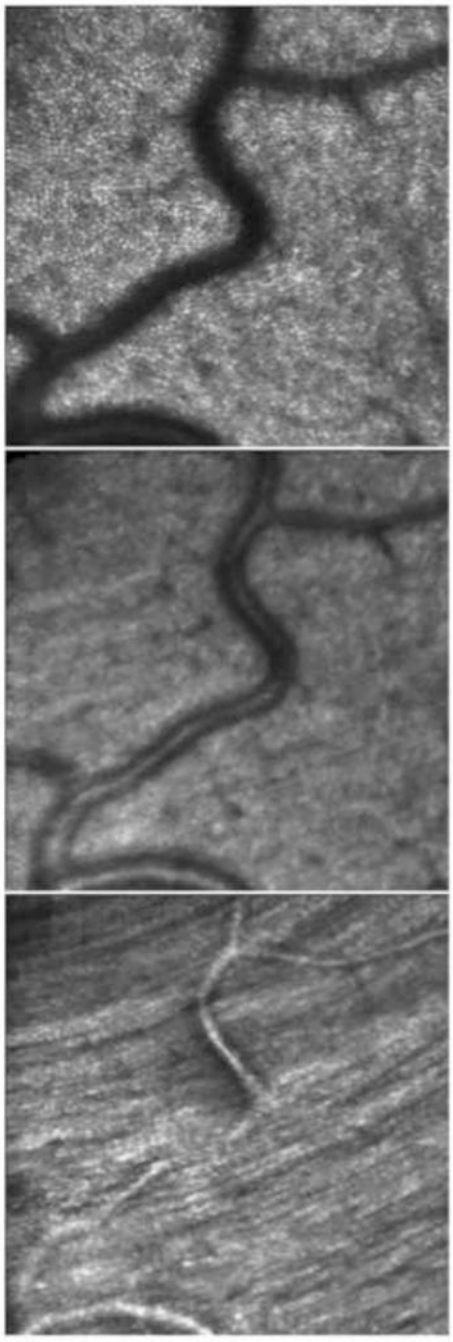

Fig. 11.

Optical sectioning of the retinal layers. In the top panel, the AOSLO is focused at the external limiting membrane and shows the mosaic of cone photoreceptors. The middle panel is an optical section of the inner retina, showing light scattered from the blood vessels. The bottom panel is an optical section with the focus on the surface of the retina, showing the striation of the nerve fiber bundles. The image is from a location about 4° inferior to the foveal center. From Roorda (2010).

NIH-PA Author Manuscript

NIH-PA Author Manuscript

NIH-PA Author Manuscript

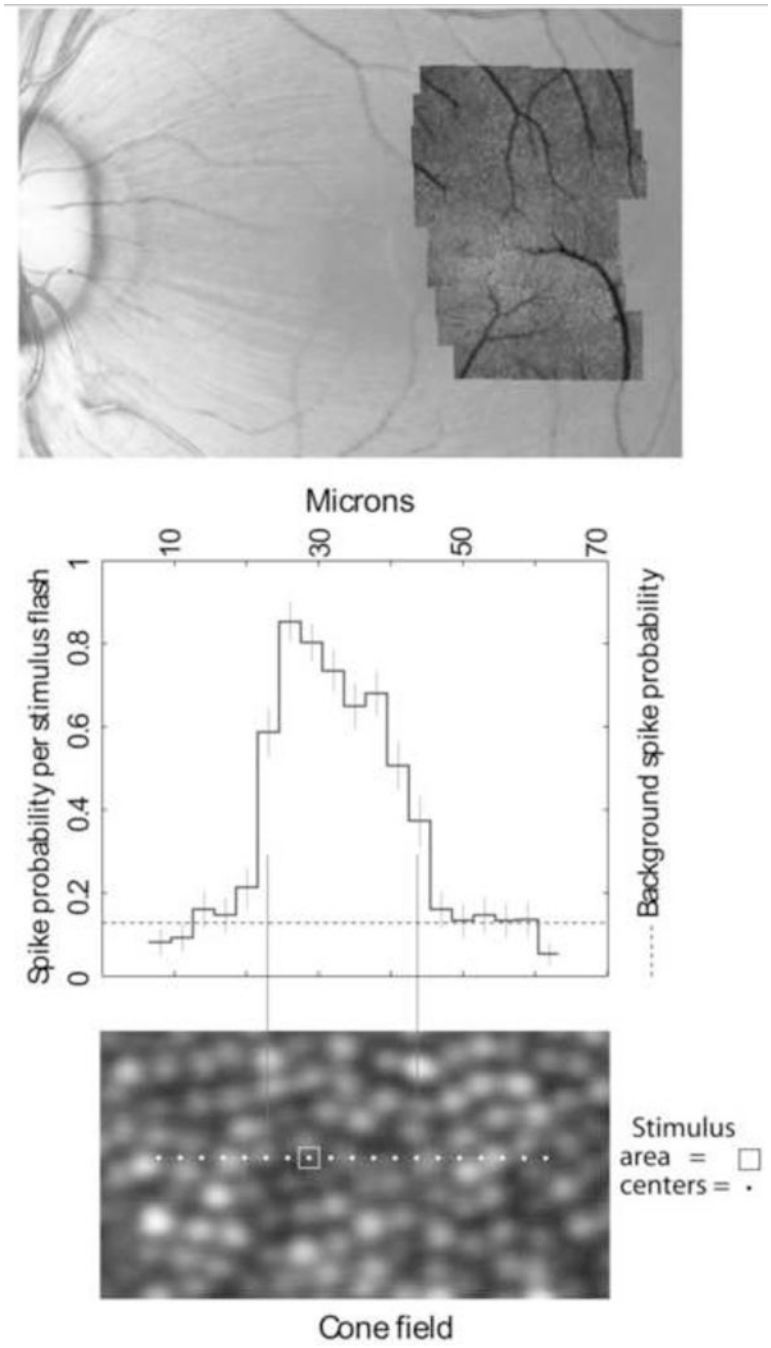

Fig. 12.

Mapping single cone cell inputs to the receptive fields of LGN cells recorded with a microelectrode in the monkey. Upper panel: color fundus photograph of macaque retina with an AOSLO montage overlay. The red dot indicates the location of the receptive field that is shown in the two lower panels. The lower panel shows the exact locations of the test areas. The central plot shows the probability that each stimulus flash will produce a neural spike (Adapted from Sincich et al., 2009). From Roorda (2010).

NIH-PA Author Manuscript

NIH-PA Author Manuscript

NIH-PA Author Manuscript

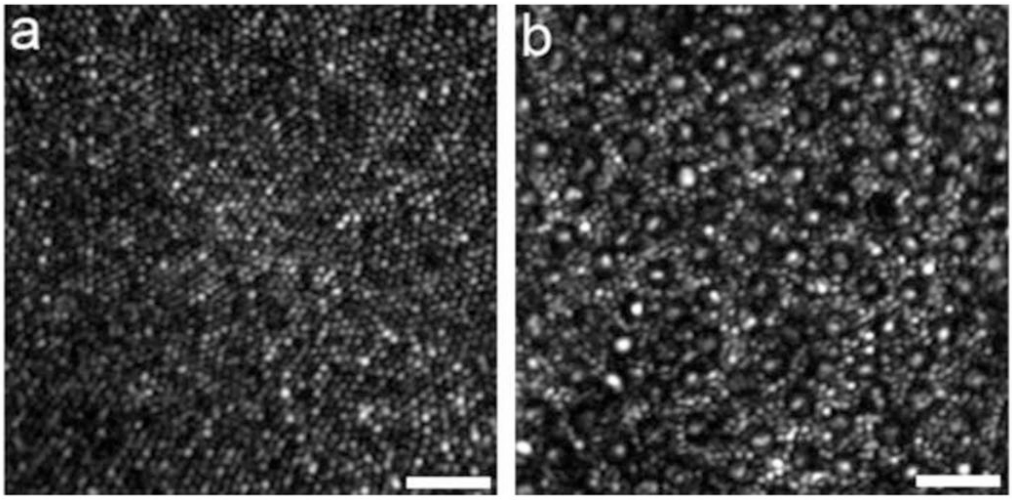

Fig. 13.

High-resolution images of the smallest photoreceptors obtained with the new Rochester AOSLO. (a) The complete foveal cone mosaic. (b) The complete peripheral photoreceptor mosaic showing both rods and cones, imaged at 101 temporal and 11 inferior. Scale bars are 20 microns. From Rossi et al. (2011).

NIH-PA Author Manuscript

NIH-PA Author Manuscript

NIH-PA Author Manuscript

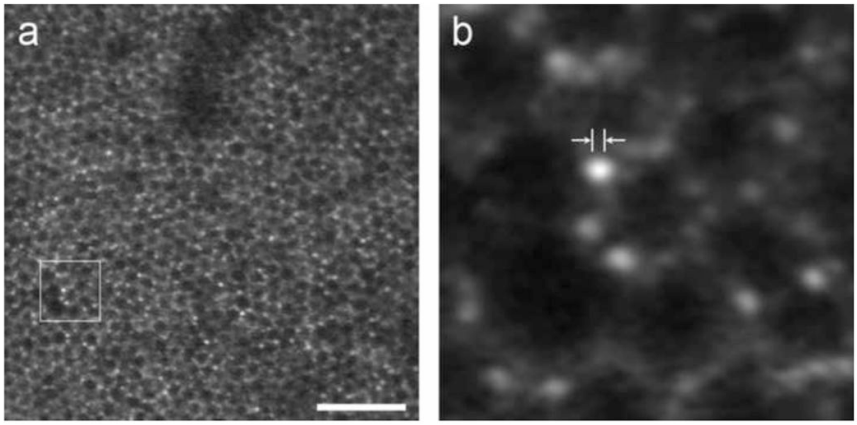

Fig. 14.

Retinal pigment epithelium and individual lipofuscin granules revealed in FAOSLO. (a) Individual RPE cells imaged using FAOSLO in macaque. Scale bar is 100 microns. (b) Outlined region from a showing individual lipofuscin granules; distance between arrowheads is 2 microns, on the order of the size expected for RPE granules. From Rossi 2011.

NIH-PA Author Manuscript

NIH-PA Author Manuscript

NIH-PA Author Manuscript

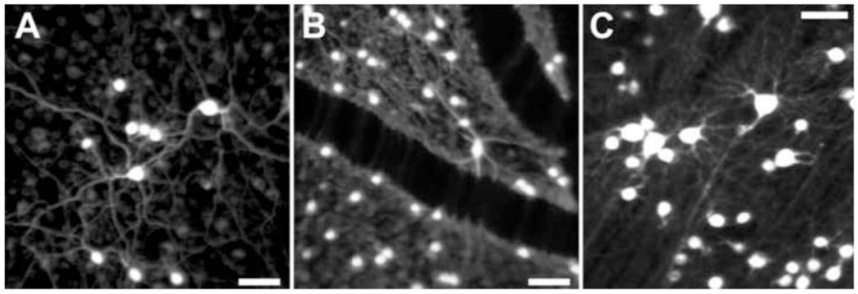

Fig. 15.

Fluorescence AOSLO images of primate retinal ganglion cells in vivo A), B) and C) Fluorescence AOSLO imaging revealed the morphology of retinal ganglion cells labeled with fluorophore (rhodamine dextran) in living monkey eye. The transverse resolution of the images is fine enough to resolve the individual dendrites. The fluorophore was introduced into the ganglion cells through retrograde labeling via injections in the lateral geniculate nucleus (LGN). Scale bar of 50 μm in all panels. [Panels A and C, Reproduced from Gray DC, Wolfe R, Gee BP, et al. (2008) In vivo imaging of the fine structure of rhodamine-labeled macaque retinal ganglion cells. Invest Ophthalmol Vis Sci 49:467-473, their Figures 1 and 5, with permission from Association for Research in Vision and Ophthalmology (Copyright 2008).]

NIH-PA Author Manuscript

NIH-PA Author Manuscript

NIH-PA Author Manuscript

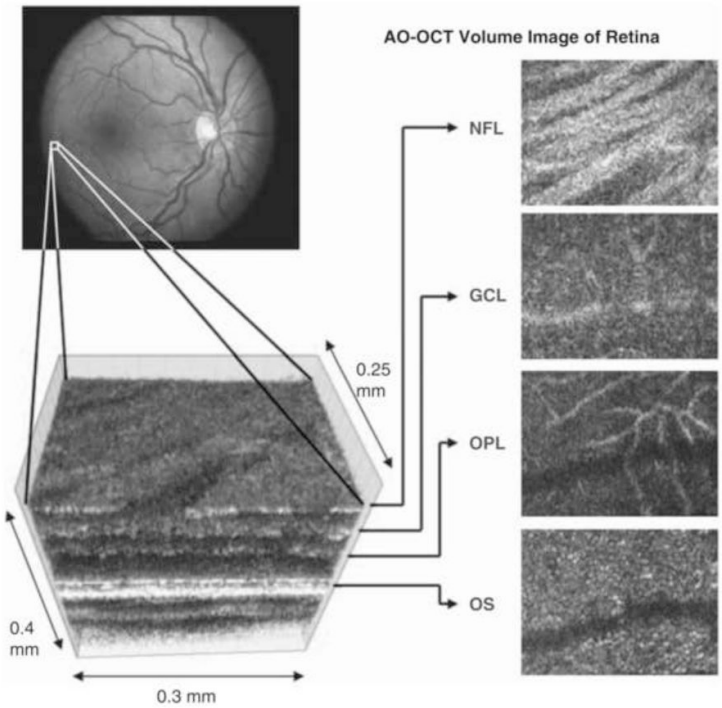

Fig. 16.

AO–OCT volume acquired over a 1deg retinal region located temporal of the fovea, as illustrated by the rectangle in the fundus photograph. The images on the right are en face views of particular retinal layers extracted from the AO–OCT volume. Retinal layers from top to bottom are: nerve fiber layer (NFL), ganglion cell layer (GCL), outer plexiform layer (OPL), and outer segment layer of photoreceptors (OS). (from Miller, 2011)

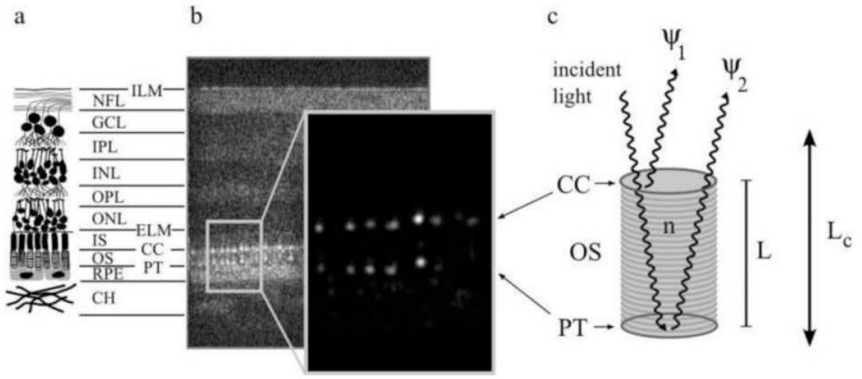

Fig. 17.

The reflective structure of the retina showing the two bright reflections especially from the cone photoreceptors that are the basis for cellular interferometry.

(a) A diagram depicting the major layers of the neural retina, consisting of the inner limiting membrane (ILM), nerve fiber layer (NFL), ganglion cell layer (GCL), inner plexiform layer (IPL), inner nuclear layer (INL), outer plexiform layer (OPL), outer nuclear layer (ONL), external limiting membrane (ELM), the inner segments (IS) and outer segments (OS) (which make up the photoreceptor layer), the connecting cilia (CC) and posterior tip (PT) layers (which bound the outer segment), the retinal pigment epithelium (RPE), and the choroid (CH). (b) An AO-OCT B-scan (log intensity), showing a cross-section of the full retinal thickness, aligned with the layers depicted in (a), and an enlarged view (linear intensity) of the cone outer segments. While OCT images are typically shown in log intensity, the linear intensity view of the outer segments demonstrates vividly that the bulk of the cone reflection originates at the CC and PT layers: the bright, patterned reflections at the CC and PT layers are the most visible structures in the linear intensity image; their peak intensity is more than two orders of magnitude greater than the average intensity of all other layers in the image. Each distinct reflection in the pattern represents a single cone cell. (c) A model of light propagation through the OS. Two bright reflections (ψ_1 and ψ_2) originate from the CC and PT layers, creating a biological interferometer in the retina that is sensitive to small ($\ll \lambda$) changes in the outer segment length L whenever the temporal coherence length of the illumination source L^c is longer than L. From Jonnal et al. (2010)

NIH-PA Author Manuscript NIH-PA Author Manuscript NIH-PA Author Manuscript

NIH-PA Author Manuscript
NIH-PA Author Manuscript
NIH-PA Author Manuscript

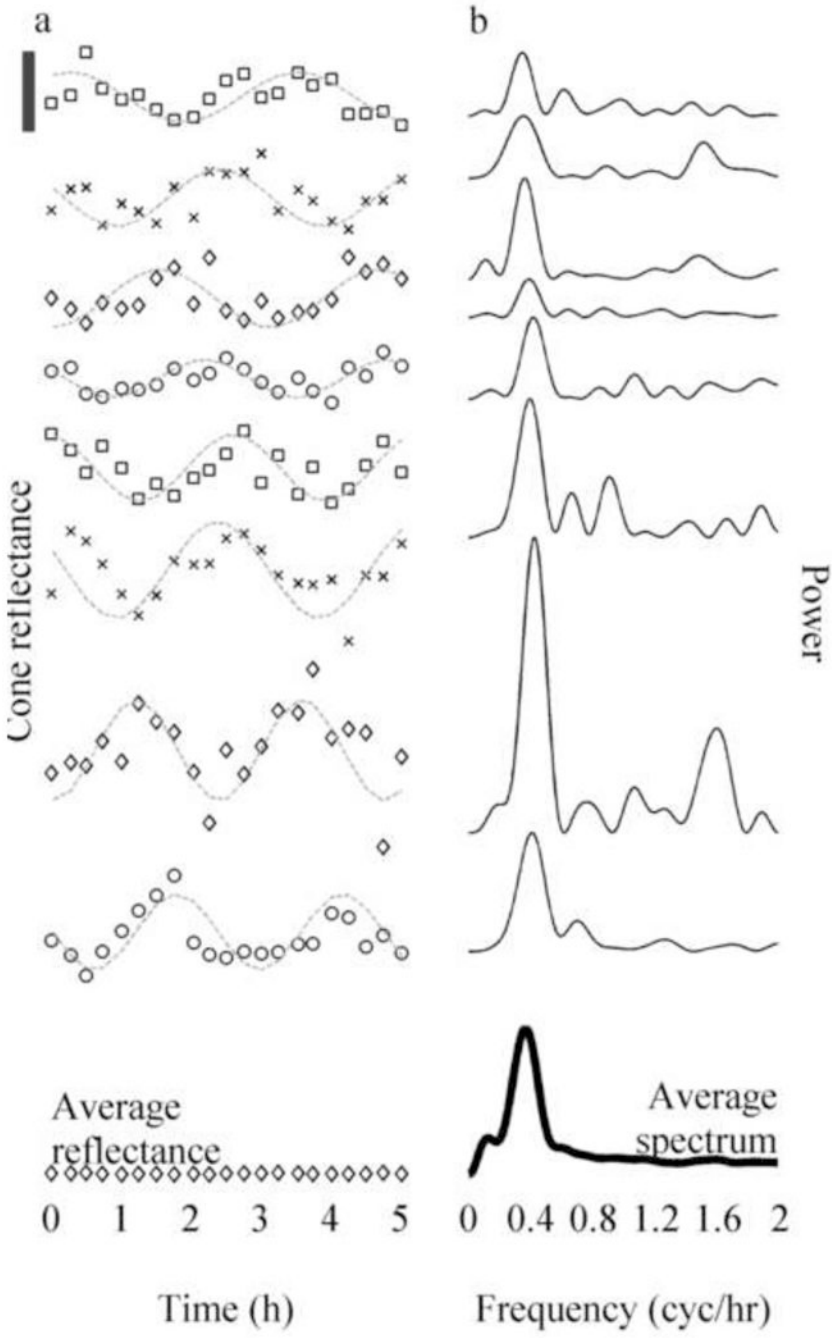

Fig. 18.

Cone reflectances and their power spectra (plots offset vertically for ease of viewing). (a) Reflectance as a function of time of eight sample cones taken from trial 4. Superimposed on each plot is a cosine fit (gray line). The black bar in the upper left shows 1/10th of the average DC component, I_0, of cone reflectance. The oscillation of reflectance in all cones had a visible period of 2.5 – 3 hours, while the amplitudes and phases appeared to vary randomly. At the bottom is a plot of the average reflectance of all cones (diamonds), nearly flat (contrast 0.18%), which is predicted by the model shown in Fig. 1(c) and Eq. (1). (b) Power spectra of mean-subtracted cone reflectance traces shown in a, and the average spectrum of all 1626 cones (dark line). Most cones in this trial had a visible peak in the

power spectrum around 0.37 cyc/hr, and this peak is visible in the average power spectrum as well. Similar peaks were seen in power spectra of individual cones, and the average power spectrum, in all trials in which the long coherence source was used (these frequencies are summarized in Table 1). When the short coherence source was used, neither the power spectra of individual cones nor the average power spectrum showed comparable peaks. From Jonnal et al. (2010).

NIH-PA Author Manuscript
NIH-PA Author Manuscript
NIH-PA Author Manuscript

NIH-PA Author Manuscript

NIH-PA Author Manuscript

NIH-PA Author Manuscript

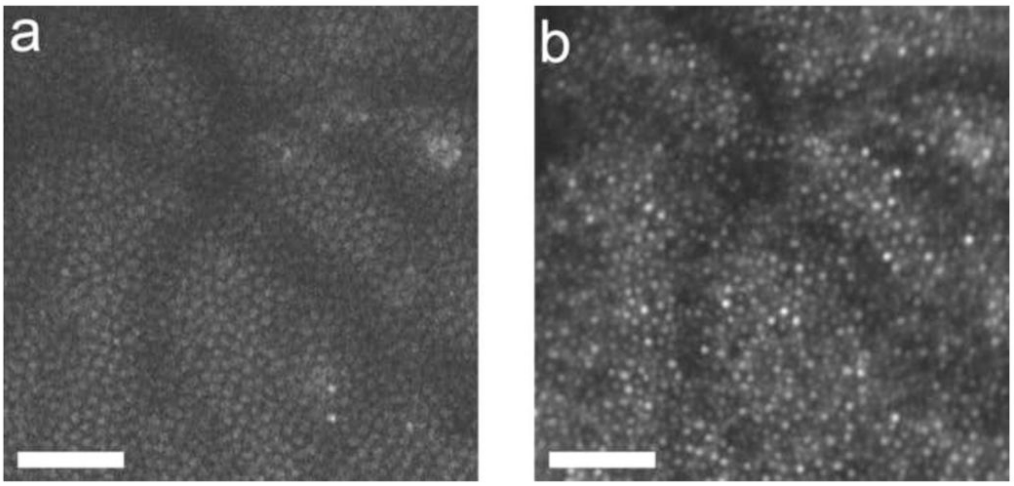

Fig. 19.

A. two-photon image of the cone mosaic in the living primate retina at 2.5 deg superior retina using 730 nm illumination from a Ti-Sapph laser with a pulse width of less than 70 fs. B. Reflectance image of the cone mosaic at the same location using 790 nm light. The bright spots in both images correspond, confirming the cone mosaic as the origin of the two photon signal. Scale bar, ?0 μm.